Monthly Notices
of the
ROYAL ASTRONOMICAL SOCIETY

MNRAS **472,** 3887–3904 (2017)
Advance Access publication 2017 August 30

doi:10.1093/mnras/stx2225

Kinematics of OB-associations in *Gaia* epoch

A. M. Mel'nik★ and A. K. Dambis

Sternberg Astronomical Institute, Lomonosov Moscow State University, Universitetskii pr. 13, Moscow 119991, Russia

Accepted 2017 August 23. Received 2017 August 23; in original form 2017 April 11

ABSTRACT

We use stellar proper motions from the *Tycho-Gaia* Astrometric Solution (TGAS) catalogue to study the kinematics of OB-associations. The TGAS proper motions of OB-associations generally agree well with the Hipparcos proper motions. The parameters of the Galactic rotation curve obtained with TGAS and Hipparcos proper motions agree within the errors. The average one-dimensional velocity dispersion inside 18 OB-associations with more than 10 TGAS stars is $\sigma_v = 3.9\,\mathrm{km\ s^{-1}}$, which is considerably smaller, by a factor of 0.4, than the velocity dispersions derived from Hipparcos data. The effective contribution from orbital motions of binary OB-stars into the velocity dispersion σ_v inside OB-associations is $\sigma_b = 1.2\,\mathrm{km\,s^{-1}}$. The median virial and stellar masses of OB-associations are equal to 7.1×10^5 and 9.0×10^3 $\mathrm{M_\odot}$, respectively. Thus, OB-associations must be unbound objects, provided they do not include a lot of dense gas. The median star-formation efficiency is $\epsilon = 2.1$ per cent. Nearly one-third of stars of OB-associations must lie outside their tidal radius. We found that the Per OB1 and Car OB1 associations are expanding with the expansion started in a small region of 11–27 pc 7–10 Myr ago. The average expansion velocity is $6.3\,\mathrm{km\ s^{-1}}$.

Key words: Galaxy: kinematics and dynamics – open clusters and associations: general – open clusters and associations: individual: Per OB1, Car OB1 – stars: formation.

1 INTRODUCTION

Galactic astronomy is on the threshold of a new era of high precision proper motions with the recent first *Gaia* data release (*Gaia* DR1; Gaia Collaboration et al. 2016b) from the European Space Agency (ESA). *Gaia* DR1 contains the *Tycho-Gaia* Astrometric Solution (TGAS; Michalik, Lindegren & Hobbs 2015; Lindegren et al. 2016) that provides positions, parallaxes and proper motions for about 2 million stars using the 24 yr time difference between Hipparcos (ESA 1997; Hog et al. 2000) and *Gaia* (Gaia Collaboration et al. 2016a) observations.

The term 'O-association' was first introduced by Ambartsumian (1949) and it implies stellar systems with enhanced density of O-stars. The sizes of OB-associations differ from 10 pc (Cyg OB2) to 500 pc (Cep OB1), although the sky-plane sizes of 90 per cent of them do not exceed 200 pc (Blaha & Humphreys 1989). They often contain young clusters in their centres (Garmany & Stencel 1992) and sometimes have several centres of concentration (Mel'nik & Efremov 1995). The catalogue compiled by Blaha & Humphreys (1989) includes 91 OB-associations located within 3.5 kpc from the Sun. This catalogue may also include several young open clusters because it is difficult to make a clear distinction between OB-associations and young open clusters. Though, OB-associations have, on average, larger sizes: 80 per cent of them are larger than $d > 20$ pc. Moreover, OB-associations are less centrally concentrated than young open clusters.

There are several partitions of high-luminosity stars (OB-stars and red supergiants) into OB-associations (Humphreys & McElroy 1984; Blaha & Humphreys 1989; Garmany & Stencel 1992; Mel'nik & Efremov 1995). Garmany & Stencel (1992) divided young stars into OB-associations in the sector of Galactic longitudes 55°–150°. Mel'nik & Efremov (1995) used cluster analysis method to identify the densest and most compact parts of OB-associations, but these groups include only few stars with known kinematical data. Both lists of OB-associations are based on photometric data obtained by Blaha & Humphreys (1989). Here, we consider the partition of Blaha & Humphreys (1989) as the most universal.

The catalogue by Blaha & Humphreys (1989) includes the massive end of the stellar population of OB-associations. In some other studies (for example, de Zeeuw et al. 1999), the authors are concerned with the entire stellar population and also consider smaller scales, such as subgroups within larger OB-associations.

OB-associations are supposed to form in giant molecular clouds (Elmegreen 1983; Zinnecker & Yorke 2007, and references therein). The diameters and masses of giant molecular clouds lie in the range of 10–80 pc and 10^5–2×10^6 $\mathrm{M_\odot}$ (Sanders, Scoville & Solomon 1985), respectively. The catalogue of Galactic giant molecular clouds is expected to be essentially complete at $M > 3 \times 10^5$ $\mathrm{M_\odot}$ (Solomon et al. 1987; Solomon & Rivolo 1989). There is a lot of evidence that giant molecular clouds

★ E-mail: anna@sai.msu.ru

are close to virial equilibrium (Larson 1981; Krumholz, Matzner & McKee 2006).

The efficiency of star formation, ϵ, determined as the ratio of the stellar mass of OB-association with the gaseous mass of its parent giant molecular clouds usually lies in the range of 0.1–10 per cent (Myers et al. 1986; Evans et al. 2009; Garcia et al. 2014). The low efficiency of star formation can be explained by two different ways: through destruction of molecular clouds by the radiation of high-luminosity stars (e.g. Elmegreen 1983; Franco, Shore & Tenorio-Tagle 1994; Colin, Vazquez-Semadeni & Gomez 2013) and through supersonic turbulence and magnetic fields preventing global collapse of the cloud (Mac Low & Klessen 2004; McKee & Ostriker 2007).

Blaauw (1964) found the expansion of OB-associations by analysing ground-based proper motions of their member stars. Brown, Dekker & de Zeeuw (1997) simulated the expansion of OB-associations to check methods for deriving their kinematic age – the time in the past when the OB-association had minimal size. Madsen, Dravins & Lindegren (2002) find some evidence for expansion in Sco OB2 by comparing spectroscopic radial velocities with values derived from the hypothesis that members of the OB-association share the same velocity vector. Although the estimated expansion velocities of OB-associations decrease with growing accuracy of proper motions, the expansion of these systems is expected in many scenarios of star formation.

The mass-loss in a gas cloud due to thermal pressure of H II regions (McKee 1989; Kim, Kim & Ostriker 2016) can make the newly formed stellar group unbound. If mass is ejected from the system within a time comparable to the crossing time, then the system becomes unbound after 50 per cent mass-loss (Hills 1980). However, more accurate treatment of relaxation processes shows that the system can form an expanding OB-association with a bound cluster in the centre (Tutukov 1978; Kroupa, Aarseth & Hurley 2001; Boily & Kroupa 2003a,b; Vine & Bonnell 2003; Baumgardt & Kroupa 2007).

We study the kinematics of OB-associations using the stellar proper motions from the TGAS catalogue (Michalik et al. 2015). The high precision of TGAS proper motions makes it possible to estimate the virial masses of OB-associations corresponding to the masses of their parent molecular clouds, and examine the expansion of OB-associations at present time.

In Section 2, we investigate the motions of OB-associations as single entities: we derive the parameters of the Galactic rotation curve and study the residual velocities and the motion along the z-axis. In Section 3, we study internal properties of OB-associations: we determine their velocity dispersions, virial and stellar masses, estimate the star formation efficiency and tidal radii. We consider the expansion of OB-associations in Section 4 and formulate the main conclusions in Section 5.

2 MOTIONS OF OB-ASSOCIATIONS IN THE GALAXY

2.1 Kinematic data of stars in OB-associations

We calculate the median proper motions of OB-associations using TGAS proper motions of individual stars (Michalik et al. 2015). On the whole, OB-associations identified by Blaha & Humphreys (1989) include 500 stars with known TGAS proper motions. For comparison, Hipparcos catalogue contains 774 star members of OB-associations. The lack of TGAS proper motions mostly concerns nearby OB-associations, which contain bright stars ($m_v < 7^m$). Determining astrometric parameters of bright stars requires additional calibrations, and for this reason, TGAS lacks many bright stars from nearby OB-associations. For example, OB-association Ori OB1 includes 59 stars with known Hipparcos proper motions and only three stars with TGAS data. We therefore consider only proper motions of stars in OB-associations and do not use their parallaxes. It is nearby stars with the most precise parallaxes that are most important for the study of the distance scale.

The mass measurements of proper motions of blue stars became available due to the inclusion of a list of OB-stars into the Hipparcos input catalogue (de Zeeuw et al. 1999), providing very accurate first-epoch positions and hence very small TGAS proper-motion errors for OB-association members. The average error of TGAS proper motions for OB-association member stars is $\varepsilon_{\mu l} = \varepsilon_{\mu b} = 0.059$ mas yr^{-1}, which is nearly 15 times smaller than the average error of Hipparcos proper motions, 0.916 mas yr^{-1}, for OB-association stars.

Table 1 presents the average Galactic coordinates of OB-associations, l and b, the average heliocentric distances to the associations, r, the median proper motions in l- and b-directions, μ_l and μ_b, the dispersion of proper motions $\sigma_{\mu l}$ and $\sigma_{\mu b}$ and the number of stars in OB-associations with known TGAS proper motions, n_μ. To complete the kinematic data, we also give the median line-of-sight velocities, V_r, the dispersion of the line-of-sight velocities σ_{vr} and the number of stars with known line-of-sight velocities, n_{vr}, taken from the catalogue by Barbier-Brossat & Figon (2000). Table 1 also gives the total number of stars in an OB-association with known photometric measurements, N_t, used by Blaha & Humphreys (1989) to determine distances for OB-associations, $r_{\rm BH}$.

Note that the errors of the listed proper motions and line-of-sight velocities of OB-associations, $\varepsilon_{\mu l}$, $\varepsilon_{\mu b}$ and ε_{vr}, are calculated in the following way:

$$\varepsilon_{\mu l} = \frac{\sigma_{\mu l}}{\sqrt{n_\mu}}, \quad (1)$$

$$\varepsilon_{\mu b} = \frac{\sigma_{\mu b}}{\sqrt{n_\mu}}, \quad (2)$$

$$\varepsilon_{vr} = \frac{\sigma_{vr}}{\sqrt{n_{vr}}}. \quad (3)$$

The method of deriving the robust estimates of the dispersion of μ_l, μ_b and V_r inside the OB-association is also discussed in Section 3.1.

Table 2, which is available in the online version of the paper, gives the spectral, photometric and kinematic data of stars in OB-associations. It presents the name of a star, the name of the OB-association to which it is assigned by Blaha & Humphreys (1989), spectral type of the star, code of its luminosity class c_L: 2 – Ia, 4 – Iab, 6 – Ib, 8 – II, 10 – III, 12 – IV, 14 – V, where the corresponding odd numbers (1, 3,..., 13) reflect the uncertainty in its determination. Table 2 also shows Galactic coordinates l and b of a star, and the heliocentric distance r to OB-association, which it is assigned to. We also present the line-of-sight velocity of a star V_r and its error ε_{vr} taken from the catalogue Barbier-Brossat & Figon (2000). Note that we use only the individual stellar velocities V_r determined with the error $\varepsilon_{vr} \leq 10$ km s^{-1} to derive the median values of V_r and velocity dispersions σ_{vr} in OB-association. For the Hipparcos stars, we present their Hipparcos number $n_{\rm Hip}$, TGAS proper motions, μ_l and μ_b, if available, and their errors, $\varepsilon_{\mu l}$ and $\varepsilon_{\mu b}$. If a Hipparcos star is absent in the TGAS catalogue, then we give its Hipparcos proper motions and their errors; flag F indicates the source of proper motions: 'G' means TGAS and 'H' – Hipparcos. Table 2 also represents colour indexes $B-V$ and $U-B$, apparent and absolute magnitudes, m_V and M_V, and the V-band extinction,

Table 1. Line-of-sight velocities and TGAS proper motions of OB-associations.

Name	l (deg)	b (deg)	r (kpc)	N_t	V_r (km s^{-1})	σ_{vr} (km s^{-1})	n_{vr}	μ_l (mas yr^{-1})	$\sigma_{\mu l}$ (mas yr^{-1})	μ_b (mas yr^{-1})	$\sigma_{\mu b}$ (mas yr^{-1})	n_μ
SGR OB5	0.02	−1.19	2.42	31	−15.0	19.0	2	−0.35	–	−2.39	–	1
SGR OB1	7.55	−0.77	1.26	65	−10.0	12.1	37	−1.10	0.22	−1.30	0.78	13
SGR OB7	10.73	−1.57	1.39	4	−6.1	17.2	3	–	–	–	–	0
SGR OB4	12.11	−0.96	1.92	15	3.5	10.7	9	−0.24	0.79	−1.41	0.34	2
SGR OB6	14.19	1.28	1.60	5	−7.3	0.1	4	–	–	–	–	0
SER OB1	16.72	0.07	1.53	43	−5.0	20.0	17	−1.10	0.63	−0.87	0.34	6
SCT OB3	17.30	−0.73	1.33	10	3.3	17.0	8	−2.51	0.61	−1.07	0.64	3
SER OB2	18.21	1.63	1.60	18	−4.0	14.5	7	−0.98	0.11	−0.16	0.08	2
SCT OB2	23.18	−0.54	0.80	13	−11.0	20.0	6	−0.51	0.34	−0.74	0.04	4
TR 35	28.03	−0.46	2.01	9	31.0	–	1	−3.05	–	−0.93	–	1
COLL 359	29.79	12.63	0.16	1	–	–	0	–	–	–	–	0
VUL OB1	60.35	0.03	1.60	28	3.1	14.7	9	−4.98	1.10	−0.86	0.52	8
VUL OB4	60.63	−1.22	0.80	9	−2.9	7.5	3	−5.10	0.21	−1.74	0.65	2
CYG OB3	72.77	2.03	1.83	42	−9.5	9.5	30	−7.15	0.30	−0.89	0.18	16
CYG OB1	75.84	1.12	1.46	71	−13.5	10.5	34	−6.35	0.54	−0.58	0.36	12
CYG OB9	77.81	1.80	0.96	32	−19.5	8.7	10	−6.44	1.13	−1.95	1.22	5
CYG OB8	77.91	3.36	1.83	21	−21.0	11.0	9	−6.27	0.43	0.53	1.60	10
CYG OB2	80.27	0.88	1.46	15	–	–	0	−5.24	–	−0.80	–	1
CYG OB4	82.69	−7.48	0.80	2	−4.9	1.1	2	–	–	–	–	0
CYG OB7	88.99	0.03	0.63	29	−9.4	9.3	21	−2.43	3.77	−1.01	0.68	16
NGC 6991	87.58	1.42	1.39	1	−15.0	–	1	–	–	–	–	0
LAC OB1	96.71	−17.70	0.48	2	−13.6	4.2	2	–	–	–	–	0
CEP OB2	102.04	4.68	0.73	57	−17.0	6.7	36	−3.84	0.91	−0.77	1.23	34
CEP OB1	104.20	−0.94	2.78	58	−58.2	7.4	17	−4.46	0.69	−0.67	0.36	20
NGC 7235	102.78	0.77	3.18	1	–	–	0	–	–	–	–	0
CEP OB5	108.50	−2.69	1.67	6	−48.7	29.2	2	−4.17	–	−0.47	–	1
CAS OB2	111.99	−0.00	2.10	41	−50.1	11.0	7	−4.02	0.07	−0.59	0.31	5
CEP OB3	110.42	2.56	0.70	26	−22.9	3.9	18	−2.13	0.51	−1.71	0.40	13
CAS OB5	116.10	−0.50	2.01	52	−45.8	7.2	16	−3.72	0.86	−0.86	0.41	8
CEP OB4	118.21	5.25	0.66	7	−24.0	–	1	−1.84	0.05	−1.29	0.04	4
CAS OB4	120.05	−0.30	2.30	27	−37.0	8.6	7	−2.50	0.17	−0.92	0.13	6
CAS OB14	120.37	0.74	0.88	8	−15.0	7.0	4	−0.87	0.08	−1.21	0.99	2
CAS OB7	122.98	1.22	2.01	39	−50.0	1.0	4	−2.47	0.23	−0.47	0.24	7
CAS OB1	124.72	−1.73	2.01	11	−42.0	2.5	5	−1.51	0.20	−1.27	0.27	3
NGC 457	126.64	−4.43	2.01	4	−34.8	2.3	4	−1.55	0.06	−0.93	0.02	2
CAS OB8	129.16	−1.06	2.30	43	−34.6	9.9	14	−1.00	0.10	−0.61	0.15	8
PER OB1	134.70	−3.16	1.83	165	−43.2	7.0	80	−0.19	0.58	−1.23	0.36	58
CAS OB6	135.02	0.75	1.75	46	−42.6	8.1	12	−0.38	0.29	−0.74	0.47	11
CAM OB1	141.08	0.89	0.80	50	−11.0	9.4	30	0.13	1.25	−1.27	0.92	26
CAM OB3	146.99	2.85	2.65	8	−27.6	19.3	3	−0.70	–	0.35	–	1
PER OB3	146.64	−5.86	0.14	1	−2.4	–	1	–	–	–	–	0
PER OB2	160.24	−16.55	0.32	7	21.2	4.5	7	5.60	0.15	−1.16	3.89	3
AUR OB1	173.83	0.14	1.06	36	−1.9	14.0	26	2.25	0.51	−1.57	0.30	12
ORI OB1	206.94	−17.71	0.40	68	25.4	7.9	62	−0.03	2.28	−0.30	0.59	3
AUR OB2	173.33	−0.17	2.42	20	−2.6	4.9	4	0.85	0.84	−0.79	0.30	2
NGC 1893	173.60	−1.70	2.90	10	–	–	0	–	–	–	–	0
NGC 2129	186.45	−0.11	1.46	3	16.8	7.5	3	1.90	–	−0.91	–	1
GEM OB1	188.98	2.22	1.21	40	16.0	5.0	18	1.53	0.39	−0.56	0.31	6
MON OB1	202.10	1.08	0.58	7	23.4	13.0	7	0.27	0.32	−1.62	0.18	4
MON OB2	207.46	−1.65	1.21	32	22.3	12.5	26	−1.10	0.22	−1.31	0.47	10
MON OB3	217.65	−0.44	2.42	4	27.0	–	1	–	–	–	–	0
CMA OB1	224.58	−1.56	1.06	17	34.3	16.2	8	−2.93	0.78	−1.93	1.15	7
NGC 2414	231.09	1.01	3.18	15	67.2	–	1	−1.94	–	−0.50	–	1
COLL 121	238.45	−8.41	0.55	13	29.6	7.0	10	−4.73	1.77	−1.53	0.37	3
NGC 2362	237.87	−5.92	1.21	9	30.0	14.0	6	–	–	–	–	0
NGC 2367	235.65	−3.84	2.20	5	37.0	9.0	4	−3.11	–	−0.66	–	1
NGC 2439	245.27	−4.08	3.50	23	62.7	–	1	−4.27	0.43	−0.54	0.18	10
PUP OB1	243.53	0.16	2.01	22	77.0	–	1	−3.66	0.11	−0.94	1.64	3
PUP OB2	244.61	0.58	3.18	13	–	–	0	–	–	–	–	0
COLL 140	244.47	−7.33	0.29	6	10.3	6.6	5	−7.56	1.23	−4.45	1.55	2

Table 1 – *continued*

Name	l (deg)	b (deg)	r (kpc)	N_t	V_r (km s^{-1})	σ_{vr} (km s^{-1})	n_{vr}	μ_l (mas yr^{-1})	$\sigma_{\mu l}$ (mas yr^{-1})	μ_b (mas yr^{-1})	$\sigma_{\mu b}$ (mas yr^{-1})	n_μ
PUP OB3	253.89	− 0.25	1.46	3	–	–	0	–	–	–	–	0
VELA OB2	262.08	− 8.52	0.39	13	24.0	9.7	13	−9.73	0.32	−4.88	2.97	2
VELA OB1	264.84	− 1.41	1.46	46	23.0	4.3	18	−6.78	1.07	−1.69	0.25	7
CAR OB1	286.45	− 0.46	2.01	126	−5.0	8.2	39	−8.08	0.74	−0.81	0.24	15
TR 16	287.25	− 0.25	2.10	18	−1.0	3.3	5	−7.20	0.55	−0.94	0.38	2
TR 14	287.37	− 0.47	2.78	5	−10.0	–	1	–	–	–	–	0
TR 15	287.65	− 0.42	3.04	2	–	–	0	–	–	–	–	0
COLL 228	287.57	− 0.98	2.01	15	−13.0	9.0	9	−6.92	–	−1.64	–	1
CAR OB2	290.39	0.12	1.79	59	−8.2	8.5	22	−6.62	0.23	−1.09	0.27	10
NGC 3576	291.33	− 0.61	2.53	5	−17.0	9.0	2	–	–	–	–	0
CRU OB1	294.87	− 1.06	2.01	76	−5.3	8.9	33	−6.28	0.32	−0.88	0.21	17
NGC 3766	294.11	− 0.02	1.53	12	−15.6	0.7	2	−6.76	0.01	−1.10	0.09	2
CEN OB1	304.14	1.44	1.92	103	−19.0	14.5	32	−4.89	0.57	−1.01	0.21	28
HOGG 16	307.51	1.39	1.46	5	−35.0	8.5	3	−3.70	0.01	−1.09	0.24	2
R 80	309.37	− 0.41	2.90	2	−38.2	–	1	–	–	–	–	0
NGC 5606	314.87	0.99	1.53	5	−37.8	1.8	3	−5.60	0.04	−0.85	0.01	2
CIR OB1	315.47	− 2.76	2.01	4	–	–	0	–	–	–	–	0
PIS 20	320.39	− 1.49	3.18	6	−49.0	–	1	−4.98	–	−0.20	-	1
NOR OB1	328.05	− 0.92	2.78	8	−35.6	6.5	6	−4.11	–	−0.69	–	1
NGC 6067	329.71	− 2.18	1.67	9	−40.0	2.6	8	−3.18	–	−0.57	–	1
R 103	332.34	− 0.75	3.18	34	−48.0	26.0	11	−5.04	1.38	−1.52	0.73	3
R 105	333.08	1.90	1.26	4	−31.0	7.0	4	−3.04	–	0.07	–	1
ARA OB1B	337.95	− 0.85	2.78	21	−34.7	10.3	9	−2.63	0.64	−1.20	0.43	6
ARA OB1A	337.69	− 0.92	1.10	53	−36.3	20.6	8	−2.05	0.33	−2.59	0.12	5
NGC 6204	338.31	− 1.15	2.20	14	−51.0	5.8	5	–	–	–	–	0
SCO OB1	343.71	1.36	1.53	76	−28.8	17.5	28	−2.26	0.41	−0.56	0.32	8
SCO OB2	351.31	19.02	0.13	10	−4.1	2.3	10	–	–	–	–	0
HD 156154	351.30	1.41	2.10	4	−4.0	8.5	3	−1.05	0.10	−0.54	0.09	2
SCO OB4	352.64	3.23	0.96	11	3.0	6.3	7	−1.34	0.42	−2.70	0.29	3
TR 27	355.06	− 0.73	0.88	11	−15.8	–	1	–	–	–	–	0
M 6	356.75	− 0.87	0.37	1	−6.4	–	1	–		–	–	0

A_V, that are adopted from the catalogue by Blaha & Humphreys (1989).

We reduced the heliocentric distances to OB-associations derived by Blaha & Humphreys (1989), $r_{\rm BH}$, to the short distance scale, $r = 0.8\,r_{\rm BH}$ (Sitnik & Mel'nik 1996; Dambis, Mel'nik & Rastorguev 2001; Mel'nik & Dambis 2009). We also correct the absolute stellar magnitudes obtained by Blaha & Humphreys (1989), $M_{V({\rm BH})}$, to bring them on to the short distance scale $M_V = M_{V({\rm BH})} + \Delta m$, where $\Delta m = -5\log 0.8 = 0.485^m$.

2.2 Comparison TGAS and Hipparcos proper motions of OB-associations

We compare the median proper motions μ_l and μ_b of OB-associations derived from data of Hipparcos and TGAS catalogues. Only 56 OB-associations containing at least two stars with known proper motions are considered. Fig. 1 shows the correlation between the Hipparcos and TGAS proper motions. The vast interval spanned by μ_l values, [−10,+6] mas yr^{-1}, is due to differential Galactic rotation. The distribution of proper-motion components μ_b is more compact, reflecting small motions perpendicular to the Galactic plane. Two associations with large negative μ_b (Coll 140 and Vela OB2) are located close to the Sun, $r = 0.3$ and 0.4 kpc, so their large negative proper motions translate into the velocities of only −7 and −9 km s^{-1}. The μ_b proper-motion components are mostly negative reflecting the positive velocity of the solar motion perpendicular to the Galactic plane, w_0, which is equal to about +7 km s^{-1}. The root-mean-square (rms) difference of TGAS and Hipparcos proper motions is the same for l- and b-direction and equal to $\sigma_\mu = 0.67$ mas yr^{-1}. This value is comparable to the average error of proper motions of OB-stars in the Hipparcos catalogue, 0.916 mas yr^{-1}. Thus, the mean difference of velocities calculated at the mean heliocentric distance of OB-associations ($r = 1.5$ kpc) is $\Delta v = 4.7$ km s^{-1}.

2.3 Galactic rotation curve

We determine the parameters of the Galactic rotation curve assuming to a first approximation that OB-associations move in circular orbits in accordance with Galactic differential rotation. The method of the determination of the parameters of the rotation curve is described in detail in Mel'nik & Dambis (2009).

Briefly, we expand the angular rotation velocity $\Omega(R)$ into a power series in $R - R_0$ to the second order and determine values of three parameters of the rotation curve: the angular velocity at the solar distance Ω_0 as well as the first and second derivatives of $\Omega(R)$ taken at the solar distance, Ω_0' and Ω_0'', respectively. We also determine the solar velocity components u_0 and v_0 with respect to the centroid of OB-associations in the direction towards the Galactic Centre and in the sense of Galactic rotation, correspondingly.

We use two samples of OB-associations (denoted as samples 1 and 2). Sample 1 includes objects whose median line-of-sight velocities V_r or proper motions μ_l were derived from the data for at least two member stars, whereas sample 2 is based on the velocities and proper motions obtained from the data for at least five member stars. Sample 1 provides 70 and 56 equations for V_r and μ_l,

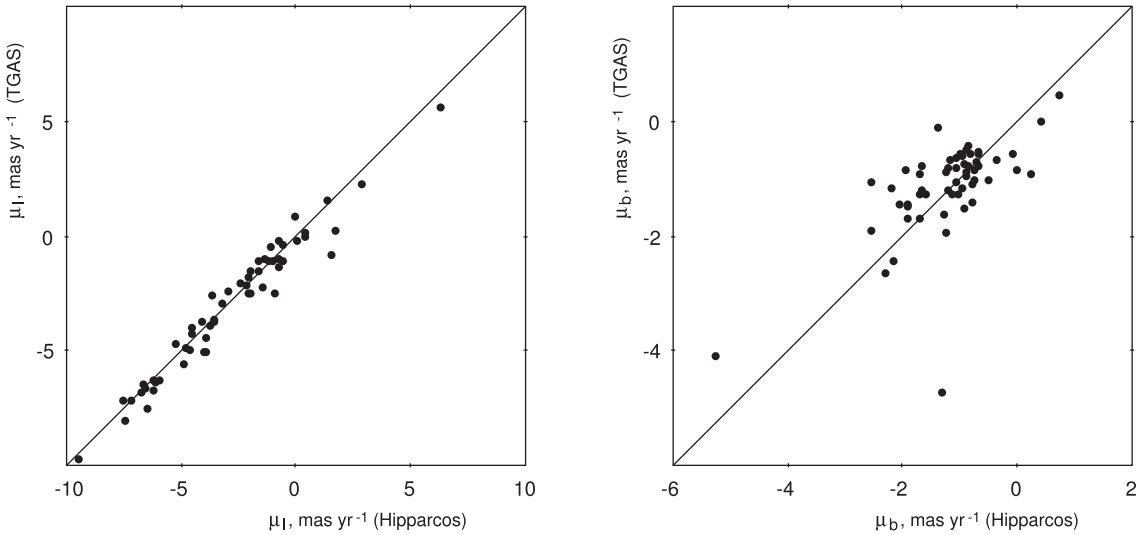

Figure 1. Comparison of proper motions μ_l and μ_b of OB-associations derived from data of Hipparcos and TGAS catalogues. Only 56 OB-associations containing at least two stars with known proper motions are considered. Note that the left and right images have different scales. The rms deviation of TGAS and Hipparcos proper motions is the same for l- and b-direction and equal to $\sigma_\mu = 0.67$ mas yr^{-1}.

Table 3. Parameters of the rotation curve.

Sample	Ω_0 (km s^{-1}) (kpc^{-1})	Ω_0' (km s^{-1}) (kpc^{-2})	Ω_0'' (km s^{-1}) (kpc^{-3})	u_0 (km s^{-1})	v_0 (km s^{-1})	A (km s^{-1}) (kpc^{-1})	σ_0 (km s^{-1})	$N_{\rm eq}$
1 ($n_{vr} \geq 2$, $n_\mu \geq 2$)	31.08	−4.75	1.11	7.27	10.63	17.83	7.42	126
	±0.86	±0.18	±0.22	±1.01	±1.33	±0.68		
2 ($n_{vr} \geq 5$, $n_\mu \geq 5$)	31.31	−4.68	1.17	7.16	12.68	17.54	7.69	82
	±1.06	±0.22	±0.31	±1.28	±1.77	±0.86		

respectively. Sample 2 gives 50 equations for V_r and 32 equations for μ_l. We solve the equations for the line-of-sight velocities and proper motions jointly and use weight factors to allow for observational errors and 'cosmic' velocity dispersion (see also Dambis, Mel'nik & Rastorguev 1995; Mel'nik, Dambis & Rastorguev 1999, 2001). We use standard least-square method (Press at al. 1987) to solve the systems of 126 (sample 1) and 82 (sample 2) equations, which are linear in the parameters Ω_0, Ω_0', Ω_0'', u_0 and v_0.

We adopt a solar Galactocentric distance of $R_0 = 7.5$ kpc (Rastorguev et al. 1994; Dambis, Mel'nik & Rastorguev 1995; Glushkova et al. 1998; Nikiforov 2004; Feast et al. 2008; Groenewegen, Udalski & Bono 2008; Reid at al. 2009b; Dambis et al. 2013; Francis & Anderson 2014; Boehle et al. 2016; Branham 2017). Note that the particular choice of R_0 in the range of 7–9 kpc has practically no effect on the analysis of the space distribution and kinematics of stars located within 3 kpc from the Sun.

Table 3 lists the parameters of the Galactic rotation curve, Ω_0, Ω_0' and Ω_0'', and the solar motion towards the apex, u_0 and v_0, determined for samples 1 and 2. It also lists the inferred Oort constant $A = -0.5 R_0 \Omega_0'$, the standard deviation of the velocities from the rotation curve σ_0, and the number of conditional equations $N_{\rm eq}$.

We can see that the parameters of the Galactic rotation curve and solar motion to the apex derived for samples 1 and 2 agree within the errors. They also agree well with the parameters obtained for Hipparcos data (see table 2 in Mel'nik & Dambis 2009). The greatest difference between the parameters derived from TGAS and Hipparcos proper motions concerns the case of the second derivative of the angular velocity $\Omega(R)$ taken at the solar distance, Ω_0'': $\Omega_0'' = 1.11 \pm 0.22$ and 1.35 ± 0.20 km s^{-1} kpc^{-3}, respectively. Note that both TGAS and Hipparcos data yield large values for the angular velocity at the solar distance Ω_0 equal to 31.08 ± 0.86 and 30.55 ± 0.87 km s^{-1} kpc^{-1}, respectively. The $\Omega_0 = 31.08$ km s^{-1} kpc^{-1} estimate translates into a solar azimuthal velocity of $\Theta = 233$ km s^{-1}. A large Ω_0 value of 30–31 km s^{-1} kpc^{-1} is also inferred from an analysis of the motions of young open clusters with ages less than 100 Myr (Mel'nik et al. 2016) and Galactic maser sources (Reid at al. 2009a; Bobylev & Baikova 2012). However, Hipparcos proper motions of classical Cepheids yield a slightly smaller value of Ω_0, 28.8 ± 0.8 (Mel'nik et al. 2015).

Fig. 2 shows the Galactic rotation curve obtained for different young objects: OB-associations with TGAS (sample 1) and Hipparcos (Mel'nik & Dambis 2009) data, young open clusters (Mel'nik et al. 2016) and classical Cepheids (Mel'nik et al. 2015). We can see that the rotation curves calculated for OB-associations with TGAS and Hipparcos proper motions are in good agreement.

2.4 Residual velocities

The residual velocities are determined as the differences between the observed heliocentric velocities and the velocities due to the inferred rotation curve and the solar motion towards the apex ($V_{\rm res} = V_{\rm obs} - V_{\rm rot} - V_{\rm ap}$). The residual velocities characterize non-circular motions in the Galactic disc. We consider the residual velocities in the direction of the Galactic radius-vector, V_R, and in

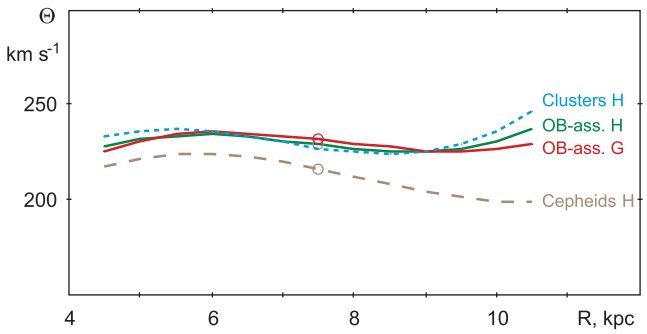

Figure 2. Galactic rotation curve obtained for different young objects: OB-associations with TGAS (sample 1) and Hipparcos data, young open clusters and classical Cepheids. The rotation curves based on TGAS and Hipparcos proper motions are labelled by the 'G' and 'H' letters, respectively. The circle shows the position of the Sun. We can see that the rotation curves obtained for OB-associations with TGAS and Hipparcos proper motions agree well with each other.

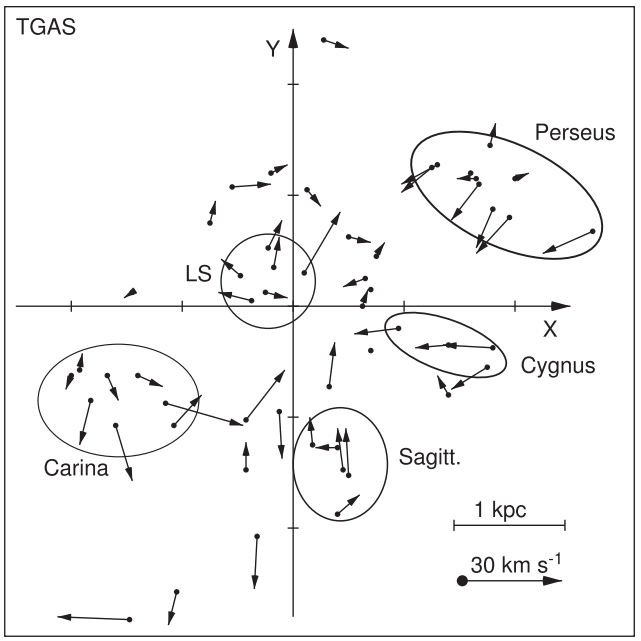

Figure 3. Distribution of the residual velocities of OB-associations in the Galactic plane. Shown are the residual velocities derived with kinematical data of at least two stars with known line-of-sight velocities and TGAS proper motions. OB-associations with residual velocities $|V_R|$ and $|V_T|$ smaller than 3 km s^{-1} are shown as the black circles without any vector. The ellipses indicate the positions of the Sagittarius, Scorpio, Carina, Cygnus, Local System (LS) and Perseus stellar–gas complexes. The x-axis points in the direction of Galactic rotation and the y-axis is directed away from the Galactic Centre. One tick interval along the x- and y-axis corresponds to 1 kpc. The Sun is at the origin.

the azimuthal direction, V_T. The velocity components V_R and V_T are positive when directed away from the Galactic Centre and in the direction of the Galactic rotation, correspondingly.

Fig. 3 shows the distribution of residual velocities of OB-associations in the Galactic plane derived with TGAS proper motions. It also shows the positions of the Sagittarius, Scorpio, Carina, Cygnus, Local System (LS) and Perseus stellar–gas complexes from the list by Efremov & Sitnik (1988). We can see that in some complexes the residual velocities V_R and V_T have a preferred direction. In the Perseus complex, the average residual velocity components are $V_R = -5.5 \pm 2.3$ and $V_T = -4.7 \pm 1.6$, whereas in the Sagittarius complex they are equal to $V_R = +7.9 \pm 2.5$ and $V_T = -1.0 \pm 2.1$ km s^{-1}. The distribution of residual velocities can be easily explained in terms of a model of the Galaxy with a two-component outer ring R_1R_2 (Mel'nik & Rautiainen 2009; Rautiainen & Mel'nik 2010; Mel'nik & Rautiainen 2011). The residual velocities in other complexes are $V_R = +6.9 \pm 2.7$ and $V_T = 1.2 \pm 3.1$ (LS), $V_R = -5.4 \pm 2.9$ and $V_T = +4.3 \pm 3.1$ (Carina) and $V_R = -4.6 \pm 1.5$ and $V_T = -11.5 \pm 1.4$ km s^{-1} (Cygnus). The rms difference of residual velocities in the stellar–gas complexes derived from TGAS and Hipparcos proper motions is less than 1 km s^{-1}.

Currently, the accuracy of measured line-of-sight velocities of stars in OB-associations is less than the accuracy of sky-plane velocities derived with TGAS proper motions. The new epoch in the study of Galactic kinematics will begin when more accurate line-of-sight velocities are obtained for young stars by the *Gaia* radial-velocity spectrometer (Gaia Collaboration et al. 2016a). Of particular interest is the direction towards the Sagittarius arm (Grosbol 2016).

2.5 Motions in the z-direction

The residual velocities in the z-direction are determined from the proper motions μ_b and line-of-sight velocities V_r:

$$V_z = 4.74\mu_b \cos b\, r + V_r \sin b + w_0, \quad (4)$$

where w_0 is the velocity of the Sun along the z-axis. Factor 4.74 transforms proper motions determined in units of mas yr^{-1} into km s^{-1} provided r is in kpc.

We selected 53 OB-associations containing at least two stars with both known line-of-sight velocities and TGAS proper motions to determine their V_z velocities and to calculate the most probable value of the solar velocity w_0, which appears to be $w_0 = 7.67 \pm 0.52$ km s^{-1}. The rms deviation of velocities in the z-direction computed with TGAS catalogue data is $\sigma_{vz} = 3.80$ km s^{-1}, which is slightly less than the scatter of vertical velocity components computed using Hipparcos data, $\sigma_{vz} = 5.0$ km s^{-1}.

Note that the absolute values of V_z velocities of OB-associations R 103 ($r = 3.2$ kpc) and Ara OB1B (2.8 kpc) decrease nearly twice: from $|V_z| = 31$ and 24 km s^{-1} when computed with Hipparcos proper motions to $|V_z| = 15$ and 8 km s^{-1} if determined using TGAS data. The other association with large V_z velocity is Cyg OB8, $V_z = +11$ km s^{-1}. Excluding these three associations changes the value of w_0 to 7.45 ± 0.38 and decreases σ_{vz} to 2.69 km s^{-1}.

Interestingly, the V_z velocity of OB-association Per OB1 is nearly zero, $V_z = -0.9$ km s^{-1}, and though Per OB1 is located ~100 pc below the Galactic plane, $b = -3.15°$, it does not move practically as a whole along the z-axis.

3 INTERNAL PROPERTIES OF OB-ASSOCIATIONS

3.1 Velocity dispersion in OB-associations with TGAS proper motions

We compare the dispersions of proper motions of stars in OB-associations obtained with Hipparcos and TGAS data (Fig. 4). Here, $\sigma_{\mu l}$ and $\sigma_{\mu b}$ are the robust estimates of the dispersions of proper motions in OB-associations derived in the following way. First, we sort the proper motions μ_l or μ_b of TGAS stars in OB-association to make rows of increasing values. Secondly, we exclude equal number

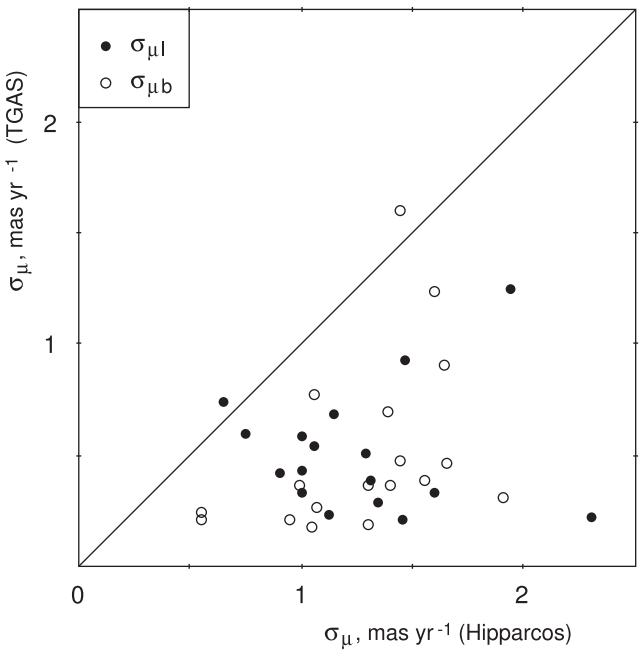

Figure 4. Comparison of the dispersions of proper motions inside OB-associations calculated with Hipparcos and TGAS data. Velocity dispersions along the l- and b-coordinate, $\sigma_{\mu l}$ and $\sigma_{\mu b}$, are shown by the black and white circles, respectively. TGAS dispersions can be seen, on average, to be smaller than the corresponding Hipparcos dispersions. The $\sigma_{\mu l} = 3.8$ mas yr^{-1} of association Cyg OB7, nearly the same when computed with TGAS and Hipparcos proper motions, is excluded from consideration.

of objects constituting the (1−0.68)/2 fraction of stars, n_μ, from the upper and lower sides of the distribution. The remaining stars make up for nearly 68 per cent of the number n_μ. The half-width of the interval in the proper-motion components spanned by the remaining stars amounts to $\sigma_{\mu l}$ or $\sigma_{\mu b}$, respectively. It is an analogue of the rms velocity dispersion, but it is less sensitive to outliers. We consider 18 OB-associations containing at least 10 stars with TGAS proper motions. When computed with TGAS data, the proper motion dispersions along l- and b-coordinates, $\sigma_{\mu l}$ and $\sigma_{\mu b}$, decrease significantly compared to the estimates obtained with Hipparcos proper motions: the reduction factor is 0.37 ± 0.006 and 0.40 ± 0.006 for l- and b-directions, respectively, or 0.39 ± 0.04 if averaged over both components. Note that $\sigma_{\mu l}$ of OB-association Cyg OB7 was excluded from consideration: it is very large, $\sigma_{\mu l} = 3.8$ mas yr^{-1}, and it is nearly the same when computed with TGAS and Hipparcos data. However, because of the small heliocentric distance of Cyg OB7, $r = 0.63$ kpc, even this very large $\sigma_{\mu l}$ value translates into a velocity dispersion of only $\sigma_{vl} = 11.4$ km s^{-1}.

We calculate the TGAS velocity dispersions, σ_{vl} and σ_{vb}, along l- and b-coordinates as follows:

$$\sigma_{vl} = 4.74 r \sigma_{\mu l}, \tag{5}$$

$$\sigma_{vb} = 4.74 r \sigma_{\mu b}. \tag{6}$$

Table 4 lists the TGAS velocity dispersions, σ_{vl} and σ_{vb}, obtained for 18 OB-associations containing at least 10 stars with TGAS proper motions, $n_\mu \geq 10$. It also provides the general information for OB-associations: the average Galactic coordinates, l and b, heliocentric (r) and Galactocentric (R) distances.

The average TGAS velocity dispersions in OB-associations are $\overline{\sigma_{vl}} = 4.3$ and $\overline{\sigma_{vb}} = 3.4$ km s^{-1}. It is currently not clear why the velocity dispersions in Cyg OB8 ($\sigma_{vb} = 13.9$ km s^{-1}) and Cyg OB7 ($\sigma_{vl} = 11.4$ km s^{-1}) are so high.

Generally, the Cygnus region is difficult to analyse because of the high concentration of bright stars in the sky plane. The large velocity dispersions in associations Cyg OB7 (σ_{vl}) and Cyg OB8 (σ_{vb}) compared to other associations can also be seen in Fig. 6.

The fact that the TGAS velocity dispersions inside OB-associations drops to 4 km s^{-1}, whereas the standard deviation, σ_0, of the velocities of OB-associations from the rotation curve remains at the level 7–8 km s^{-1} (Table 3) indicates that OB-associations identified by Blaha & Humphreys (1989) mainly include stars born from the same molecular cloud.

Due to the turbulent motions inside giant molecular clouds, the velocity dispersion inside a cloud must grow with the size S of the region considered as $\sigma_v \sim S^p$. The study by Solomon et al. (1987) suggests that power index p is close to $p \approx 0.5$. If we suppose that the velocity dispersion in a giant cloud with a diameter of 10 pc (the average size of open clusters) is 1–2 km s^{-1}, then it must be ∼3 times larger for clouds of 100 pc in diameter (the average size of OB-associations), i.e. 3–6 km s^{-1}. So the value of $\sigma_v = 4$ km s^{-1} is consistent with the properties of giant molecular clouds.

3.2 Binary stars

Mason et al. (1998) find that the majority (>59 per cent) of O-stars in clusters and OB-associations are binary. In principle, binary stars can inflate the observed velocity dispersion inside OB-associations derived with TGAS proper motions, which are calculated from the positions obtained with the time difference $T = 24$ yr. The main contribution into TGAS proper motions must be provided by binary systems with orbital periods of $P \approx 50$ yr, which corresponds to the component of the binary system moving to the opposite points of their orbit between the epochs of Hipparcos and *Gaia*.

Let us calculate the upper limit for the probable contribution of binary stars, σ_b, into the observed dispersion of TGAS proper motions inside OB-associations. For simplicity, we consider a binary system consisting of two components of mass $M_b = 10\,M_\odot$ moving in circular orbits around their common mass centre with period P. A $10\,M_\odot$-star can be considered as a representative of stars in OB-associations from the list by Blaha & Humphreys (1989): most of stars listed in the catalogue (about 2/3) have spectral types in the B0–B2 interval corresponding to the mass range of 8–15 $M_\odot$ (Hohle, Neuhäuser & Schutz 2010).

The distance between the component stars D can be estimated from Newton's gravity law:

$$\frac{M_b\, V_{\rm orb}^2}{D/2} = \frac{G\, M_b^2}{D^2}, \tag{7}$$

or, given that

$$V_{\rm orb} = \pi\, D/P, \tag{8}$$

we have

$$\frac{D^3}{P^2} = \frac{G\, M_b}{2\pi^2}, \tag{9}$$

or

$$D = \left(\frac{G}{2\pi^2}\right)^{1/3} P^{2/3}\, M_b^{1/3}. \tag{10}$$

The distance between components, D, is the maximal possible shift of the star between the two epochs of observations. However, the real displacement is smaller because the star positions at the two epochs are practically always less than the orbit diameter apart. The

Table 4. Virial and stellar masses of OB-associations, $M_{\rm vir}$ and $M_{\rm st}$, star formation efficiency ϵ.

Name	l (deg)	b (deg)	r (kpc)	R (kpc)	σ_{vl} (km s^{-1})	σ_{vb} (km s^{-1})	a (pc)	r_{td} (pc)	$M_{\rm vir}$ $M_\odot$	n_μ	$M_{\rm st}$ $M_\odot$	N_{20}	$M_{\rm g}$ $M_\odot$	ϵ 100 %
SGR OB1	7.55	−0.77	1.26	6.25	1.3	4.6	42	24	3.6×10^5	13	9.6×10^3	23	7.6×10^3	2.7
CYG OB3	72.77	2.03	1.83	7.17	2.6	1.5	26	28	0.9×10^5	16	11.7×10^3	28	1.7×10^3	13.6
CYG OB1	75.84	1.12	1.46	7.28	3.8	2.5	32	31	3.1×10^5	12	16.7×10^3	40	3.5×10^3	5.3
CYG OB8	77.91	3.36	1.83	7.34	3.7	13.9	42	24	36.8×10^5	10	7.1×10^3	17	7.4×10^3	0.2
CYG OB7	88.99	0.03	0.63	7.52	11.3	2.0	53	19	26.4×10^5	16	3.3×10^3	8	15.6×10^3	0.1
CEP OB2	101.59	4.64	0.73	7.68	3.2	4.2	45	26	6.5×10^5	34	8.3×10^3	20	9.4×10^3	1.3
CEP OB1	104.14	−0.97	2.78	8.61	9.0	4.7	178	36	94.8×10^5	20	16.7×10^3	40	576.4×10^3	0.2
CEP OB3	110.42	2.56	0.70	7.77	1.7	1.4	12	14	0.1×10^5	13	1.2×10^3	3	0.2×10^3	10.0
PER OB1	134.67	−3.15	1.83	8.88	5.0	3.1	59	48	8.2×10^5	58	36.2×10^3	87	20.9×10^3	4.4[a]
CAS OB6	135.02	0.75	1.75	8.83	2.4	3.9	78	29	7.8×10^5	11	7.9×10^3	19	49.4×10^3	1.0
CAM OB1	141.08	0.89	0.80	8.14	4.7	3.4	86	23	15.3×10^5	26	5.0×10^3	12	66.0×10^3	0.3
AUR OB1	173.83	0.14	1.06	8.55	2.6	1.5	69	22	2.2×10^5	12	3.7×10^3	9	33.9×10^3	1.7
MON OB2	207.46	−1.65	1.21	8.59	1.3	2.6	71	25	2.0×10^5	10	5.8×10^3	14	36.6×10^3	2.9
NGC 2439	245.27	−4.08	3.50	9.50	7.2	3.0	155	31	44.0×10^5	10	7.9×10^3	19	384.7×10^3	0.2
CAR OB1	286.45	−0.46	2.01	7.19	7.0	2.3	63	34	11.9×10^5	15	21.2×10^3	51	26.2×10^3	1.8[a]
CAR OB2	290.39	0.12	1.79	7.08	2.0	2.2	28	26	1.0×10^5	10	10.4×10^3	25	2.2×10^3	10.5
CRU OB1	294.87	−1.06	2.01	6.90	3.1	2.0	40	26	2.4×10^5	17	10.0×10^3	24	6.8×10^3	4.2
CEN OB1	304.14	1.44	1.92	6.62	5.2	1.9	69	32	9.1×10^5	28	21.2×10^3	51	34.4×10^3	2.3

Note. [a]Values of $M_{\rm vir}$ and ϵ for Per OB1 and Car OB1 are corrected for the expansion effect (Section 4.3)

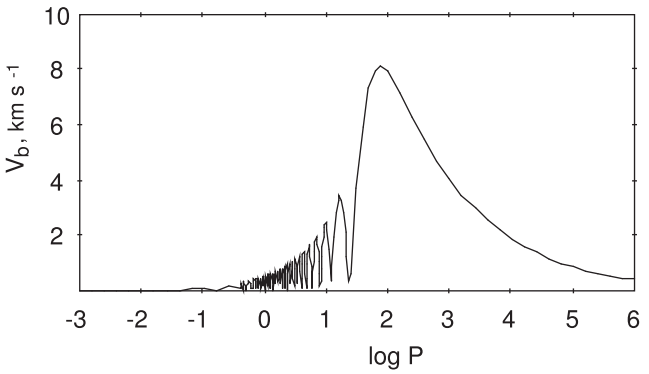

Figure 5. Dependence of the additional velocity V_b on $\log P$. Binary system considered includes two stars of mass $10\,M_\odot$ rotating on a circular orbit around their common mass centre with period P. The velocity V_b is the maximal contribution of a binary system into the TGAS velocity dispersion.

length of the chord connecting the initial and final position of the star in its circular orbit is (by law of cosines):

$$S = D\sqrt{\frac{(1-\cos(2\pi\frac{T}{P}))}{2}}. \tag{11}$$

The maximum possible extra velocity along any given direction due to the orbital displacement of this component is equal to

$$V_b = \frac{S}{T}, \tag{12}$$

or, in view of equations (10) and (11):

$$V_b = 6.0\,P^{2/3}\,M_b^{1/3}T^{-1}\sqrt{\frac{(1-\cos(2\pi\frac{T}{P}))}{2}}, \tag{13}$$

where V_b is in km s^{-1}, M_b is in solar masses, P and T are in years.

Fig. 5 shows the dependence of the maximum additional velocity V_b on $\log P$ for $M_b = 10\,M_\odot$ and $T = 24$ yr. The velocity V_b reaches maximum of 8.1 km s^{-1} at period ∼80 yr, because the radius of the orbit increases with increasing P. The decrease of V_b at larger P is caused by the fact that a star can pass only a small part of its orbit for 24-yr time interval. On the other hand, the decrease of V_b at smaller P is due to decreasing distance D between binary stars, $D \sim P^{2/3}$. The velocity V_b demonstrates oscillations with zero values corresponding to the periods $P = T/n$, where n is integer and the binary star makes a whole number of revolutions in time interval T, resulting in zero displacement D.

To estimate the effective contribution of binary stars into the velocity dispersion inside OB-association, σ_v, we should consider the fraction of multiple stars, f_b, in OB-associations, the factor measuring the average projection, f_j, of the shift S into l- or b-direction, distribution of binary periods $f_p(\log P)$, and the additional velocity due to orbital motion, $V_b^2(\log P)$, as a function of $\log P$.

Sana (2017) overviews recent estimates of the fraction of binary stars amongst OB-stars, which vary from $f_b = 0.2$ to 0.7. We adopt $f_b = 0.5$ as some average value.

If we suppose that the ensemble of the binary systems in an OB-association is oriented randomly with respect to the line of sight, then the effective value of the squared projection of the orbital displacement S_l^2 or S_b^2 on to the longitude or latitude direction, respectively, is equal to $S^2/3$, hence $f_j = 1/3$.

Aldoretta et al. (2015) show that the period distribution of massive binary stars is approximately flat in increments of $\log P$ (Öpik's law) in the interval of $\log P$ from −3 to +6. So we can suppose that $f_p = 1/9$ for unit of $\log P$.

Generally, we can write

$$\sigma_b^2 = f_b\,f_j\int_{\log P=-3}^{\log P=+6} V_b^2(\log P)\,f_p(\log P)\,d\log P. \tag{14}$$

We now use the values of $f_b = 0.5, f_j = 1/3, f_p = 1/9$ and the distribution of V_b over $\log P$ (Fig. 5) to calculate the effective contribution of binary stars into the TGAS velocity dispersion (equation 14), which appears to be $\sigma_b = 1.19$ km s^{-1}, or

$$\sigma_b = 1.19\,(M_b/10\,M_\odot)^{1/3} \tag{15}$$

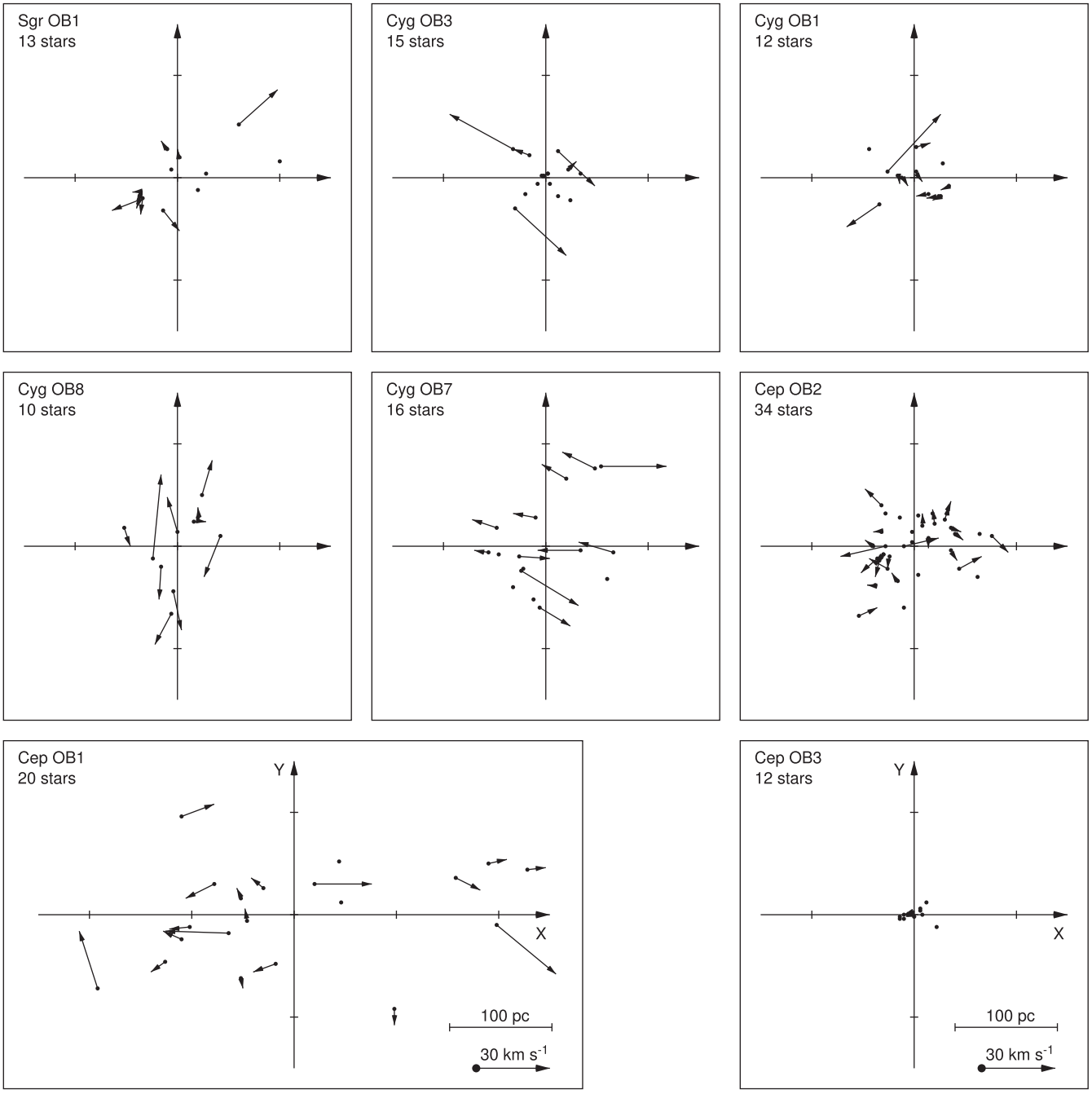

Figure 6. Distribution of the relative velocities v'_l and v'_b (equations 37 and 38) inside OB-associations with more than 10 TGAS stars. Stars with the relative velocities $|v'_l|$ and $|v'_b|$ smaller than 3 km s^{-1} are shown as black circles without any vector. The axes x and y are directed towards increasing values of Galactic coordinates l and b, respectively. All images are on the same scale. One tick corresponds to 100 pc. The Per OB1 association is not included in this panorama – we show it in a special image (Fig. 10). The Cep OB1 association is shown in a wider box because of its large extension in the l-direction. The velocity scale is shown in the bottom row.

for a binary component of mass M_b. This value is rather small compared to $\sigma_v = 4\,\mathrm{km\,s^{-1}}$ caused by turbulent motions inside giant molecular clouds.

3.3 Virial and stellar masses of OB-associations

Giant molecular clouds are supposed to be close to their virial equilibrium (Larson 1981; Krumholz et al. 2006) and therefore the velocity dispersions of stars in OB-associations must correspond to the masses of their parent giant molecular clouds. The high precision of TGAS proper motions allows estimating the virial masses of OB-associations. The virial condition between the kinetic K and potential U energies of a system is

$$2K + U = 0. \quad (16)$$

The potential energy of a uniform sphere of radius a and constant density ρ is

$$U = -\int_0^a \frac{(\frac{4}{3}G\pi\rho r^3)(4\pi\rho r^2 \mathrm{d}r)}{r} = -\frac{3GM^2}{5a}, \quad (17)$$

where M is the mass of the sphere:

$$M = \frac{4\pi a^3 \rho}{3}. \quad (18)$$

The kinetic energy of a system with one-dimensional velocity dispersion σ_v is

$$K = \frac{3M\sigma_v^2}{2}. \quad (19)$$

Hence, the virial mass of the parent giant molecular cloud can be calculated in the following way:

$$M_{\rm vir} = \frac{5a\sigma_v^2}{G}, \quad (20)$$

where σ_v and a are determined from observations.

There is no problem with observed one-dimensional velocity σ_v, it can be estimated as the average of σ_{vl} and σ_{vb}:

$$\sigma_v = (\sigma_{vl} + \sigma_{vb})/2. \quad (21)$$

However, the so-called radius a of a parent molecular cloud can be treated in different ways. We calculate a as the radius containing 68 per cent of the association member stars. Here, we consider all members of OB-associations with known photometric measurements and not just TGAS stars. We also suppose that the sizes of OB-associations have not changed significantly since the epoch of star formation. However, some OB-associations appear to be expanding, so in these cases, the radius a needs a correction (for more details, see Section 4.3).

Table 4 also gives values of $M_{\rm vir}$ and a. The median value of $M_{\rm vir}$ for 18 OB-associations considered is 7.1×10^5 M$_\odot$ that is consistent with the masses of giant molecular clouds 10^5–10^6 M$_\odot$ (Sanders et al. 1985).

Note that in our calculations of virial masses we used the values of σ_v corrected for the effect of binary stars:

$$\sigma_{\rm cor}^2 = \sigma_v^2 - \sigma_b^2. \quad (22)$$

To estimate the stellar masses of OB-associations, we use the multicomponent power-law distribution derived by Kroupa (2002). The number of stars $\mathrm{d}N(M)$ in the mass range ΔM is determined for three mass domains by the following laws:

$$\mathrm{d}N(M) = C_0 \begin{cases} C_1\, M^{-0.3} & 0.01 < M/\mathrm{M}_\odot < 0.08 \\ C_2\, M^{-1.3} & 0.08 < M/\mathrm{M}_\odot < 0.5 \\ C_3\, M^{-2.3} & 0.5 < M/\mathrm{M}_\odot < \infty. \end{cases} \quad (23)$$

The coefficients C_1, C_2 and C_3 are calculated from the continuity condition at the boundaries of the mass domains: $C_1 = 0.469$, $C_2 = 0.038$ and $C_3 = 0.019$.

We also assume that the catalogue by Blaha & Humphreys (1989) includes all stars of OB-associations with masses greater than 20 M$_\odot$ or it is essentially complete down to the absolute magnitude $M_V < -4.0^m$. To determine the mass of stars in OB-associations, we use the mass-absolute magnitude relation by Bressan et al. (2012). This relation is monotonic in the range of $-7.8 < M_V < +0.50$ and corresponds to the mass range of 3–50 M$_\odot$, which covers 99.3 per cent of OB-association stars listed in the catalogue by Blaha & Humphreys (1989). The age of the brightest OB-stars is supposed to be 4 Myr.

The value of C_0 is derived from the following calibration:

$$N_{20} = C_0 C_3 (20^{-1.3} - 50^{-1.3})/1.3, \quad (24)$$

where N_{20} is the number of stars with masses $M > 20\,\mathrm{M}_\odot$ in a particular OB-association.

Table 4 also gives the stellar masses $M_{\rm st}$ of OB-associations and the number N_{20} of stars with masses $M > 20\,\mathrm{M}_\odot$. The median value of $M_{\rm st}$ calculated for 18 OB-associations is 9.0×10^3 M$_\odot$. Note that in the case of pure Salpiter (1955) distribution, $\mathrm{d}N \sim M^{-2.35}\mathrm{d}M$, in the mass interval from 0.08 (Grossman & Graboske 1971) to 50 M$_\odot$ we obtain nearly twice greater $M_{\rm st}$ values with the median of 19×10^3 M$_\odot$.

For each OB-association from Table 4, we can estimate the average efficiency of star formation in its parent molecular cloud, which is equal to the ratio of the stellar mass to the gaseous mass of the giant cloud:

$$\epsilon = M_{\rm st}/M_{\rm vir}. \quad (25)$$

Table 4 shows that ϵ values vary from 0.1 to 13.6 per cent with the median value of 2.1 per cent that agrees with other estimates (Myers et al. 1986; Evans et al. 2009; Garcia et al. 2014).

Note that the estimates of star-formation efficiency ϵ obtained here refer to the entire volume of OB-associations, and ϵ can be smaller or larger in different parts of their parent giant molecular cloud.

3.4 Present-day mass of OB-associations and their unboundness

The fact that virial mass exceeds the stellar mass by more than 70 times supports the conclusion that OB-associations are unbound objects. Some doubts concern the gas that OB-associations could harbour inside their volumes, so the real masses of OB-associations can be conspicuously larger than those of the stellar component.

Numerical simulations demonstrate that stars with masses $M \geq 20\,\mathrm{M}_\odot$ destroy crucially molecular clouds of masses up to a few times 10^4 M$_\odot$ (Colin et al. 2013; Dale, Ercolano & Bonnell 2012).

Table 4 shows that out of the 18 OB-associations considered 9 contain more than 20 stars with masses $M \geq 20\,\mathrm{M}_\odot$. On the other hand, masses of their parent molecular clouds are 10^5–10^6 M$_\odot$, implying the average escape velocity of 12 km s^{-1}, and hence the full evaporation of gas clouds seems to be impossible.

Dale et al. (2012) simulate the star-formation processes in the molecular cloud with mass 10^6 M$_\odot$ and initial radius of 180 pc. They found that after 3 Myr of ionization the surface density Σ of the cloud is $\sim 2 \times 10^{-3}$ g cm^{-2}, which corresponds to the volume density of $\sim$1 atom cm^{-3}.

Cappa & Herbstmeier (2000) study the distribution of H I gas in the vicinity of association Per OB1. Their Fig. 2 indicates that H I surface density inside Per OB1 is $\Sigma \sim 3 \times 10^{20}$ atoms cm^{-2}. If the size of Per OB1 along the line of sight is $\sim$200 pc, then the H I volume density must be $\sim$0.5 atom cm^{-3}.

Let us suppose that the fraction of molecular gas inside the volume of OB-associations is negligible, but neutral hydrogen with the volume density $\rho_{\rm H}$ equal to 1 atom cm^{-3} can be present there. Then the upper estimate for the present-day mass of OB-association, M_t, includes the mass of the stellar component, $M_{\rm st}$, and the mass of H I possibly located inside the volume of the OB-association:

$$M_t = M_{\rm st} + M_{\rm g}. \quad (26)$$

The gas mass M_g can be estimated from the following formula:

$$M_{\rm g} = \frac{4\pi}{3} a^3 \rho_{\rm H}. \quad (27)$$

Table 4 also lists the masses of the gaseous component, $M_{\rm g}$. The median gas mass appears to be 18.3×10^3 $M_\odot$, and hence the contribution of gas to the total mass is usually comparable to the mass of the stellar component. The exception is two extremely extended OB-associations: Cep OB1 and NGC 2439, where M_g exceeds $M_{\rm st}$ by a factor of more than 30, however, even in these cases the total masses of OB-associations, $M_{\rm t}$, are nearly 10 times smaller than the corresponding virial masses, $M_{\rm vir}$.

We can thus conclude that OB-associations must be unbound objects, provided they do not contain a lot of dense gas.

3.5 Tidal radius of OB-associations

Given the known present-day masses of OB-associations, we can estimate their tidal radii, $r_{\rm td}$, at which the gravitational force produced by the OB-association equals the tidal perturbation from the Galaxy.

Let us consider the forces applied to a test particle located between the OB-association and the Galactic Centre. Subscripts 1 and 2 refer to the distances and velocities of the test particle and the centre of the OB-association, respectively. The distance between the test particle and the centre of the OB-association is $\Delta R = R_1 - R_2 < 0$. The test particle is subject to two forces working in the opposite directions: the gravity from the Galaxy, $\Omega_1^2 R_1$, and the gravity from the OB-association, $GM/(\Delta R)^2$. If the test particle is bound with the OB-association, then it rotates around the Galactic Centre at the angular velocity of the OB-association, Ω_2. Here, we ignore the velocity of the test particle due to the gravity of the OB-association. The acceleration of the test particle is equal to the sum of its centripetal acceleration, $\Omega_2^2 R_1$, and additional acceleration determined with respect to the centre of the OB-association, $\ddot{R}_1$. Newton's law gives us the following equation:

$$\ddot{R}_1 - \Omega_2^2 R_1 = \frac{GM}{(\Delta R)^2} - \Omega_1^2 R_1, \quad (28)$$

where M is the mass of the OB-association, $M = M_t$. The tidal radius, $r_{\rm td}$, is derived from the condition $\ddot{R}_1 = 0$. By assuming $\Delta R/R_2 \ll 1$, we obtain the following estimate:

$$r_{\rm td} = |\Delta R| = \left(\frac{GM}{4A\Omega}\right)^{1/3}, \quad (29)$$

where A is Oort's constant, $A = -0.5R\Omega'(R)$, at the Galactocentric distance R.

The formula for the tidal force, $T = -4A\Omega\Delta R$, can also be derived from basic equations by Goldreich & Tremaine (1980, equation 32); it is also discussed in Stark & Blitz (1978, equation 1).

We calculate the tidal radii $r_{\rm td}$ for 18 OB-associations containing at least 10 stars with TGAS proper motions. The angular velocity Ω and its first derivative Ω' at the Galactocentric radius R of each OB-association are computed based on the parameters of the rotation curve given in Table 3. The median tidal radius $r_{\rm td}$ appears to be 40 pc, which is a bit smaller than the median radius a of OB-associations, 56 pc. On average, 27 per cent of stars of OB-associations must lie outside their tidal radii and tidal perturbations from the Galaxy are essential for them.

We also calculate the minimal value of the tidal radius (Table 4) assuming that the mass of the OB-association consists of stellar component exclusively, $M = M_{\rm st}$. The tidal radii of OB-associations then drop to the values in the 14–48 pc interval with the median of 26 pc. It means that 39 per cent of member stars of OB-associations must be located outside their tidal radii.

Thus, two different estimates of tidal radii of OB-associations yield nearly the same result: $\sim 1/3$ of stars of OB-associations must lie outside their tidal radius.

4 EXPANSION OF OB-ASSOCIATIONS

4.1 Determination of the parameters of expansion/compression of OB-associations

We use TGAS proper motions to study possible expansion/compression of OB-associations in the l- and b-direction. The parameters of expansion/compression p_l and p_b are calculated from the following equations:

$$4.74\mu_l r = v_{l0} + p_l\, r \sin(l - l_0), \quad (30)$$

$$4.74\mu_b r = v_{b0} + p_b\, r \sin(b - b_0), \quad (31)$$

where v_{l0} and v_{b0} are the average velocities of the association; l_0 and b_0 are the coordinates of the centre of the association, and parameters p_l or p_b characterize expansion/compression along the l- or b-direction (positive and negative values correspond to expansion and compression, respectively).

The observed specific velocities of expansion or compression, u_l and u_b, are calculated in following way:

$$u_l = p_l\, a, \quad (32)$$

$$u_b = p_b\, a. \quad (33)$$

Note that expansion/compression of OB-associations requires some caution in interpretation: the motion of an association as a whole with the line-of-sight velocity V_r (see Table 1) can cause the effect of spurious expansion/compression. The velocity of spurious expansion/compression, e_1, caused by the line-of-sight velocity V_r is determined by the following expression:

$$e_1 = -V_r \frac{a}{r}, \quad (34)$$

where the negative line-of-sight velocities V_r produces spurious expansion, $e_1 > 0$, while positive V_r gives spurious compression, $e_1 < 0$.

Table 5 lists the parameters of observed expansion/compression, p_l and p_b, the radius of OB-associations, a, the velocity of spurious expansion/compression e_1, the observed specific velocities of expansion/compression, u_l and u_b, and the number of stars with known TGAS proper motions, n_μ. We can see that the velocity of spurious expansion/compression, e_1, can reach ~ 4 km s^{-1} (Cep OB1). So the observed velocities of expansion/compression, u_l or u_b, should be corrected for this effect:

$$\tilde{u}_l = u_l - e_1, \quad (35)$$

$$\tilde{u}_b = u_b - e_1. \quad (36)$$

The corrected velocities of expansion/compression, $\tilde{u}_l$ and $\tilde{u}_b$, are listed in Table 5 as well. Further, we will discuss only velocities, $\tilde{u}_l$ and $\tilde{u}_b$, determined at $P > 2.5\sigma$ confidence level, which are underlined in Table 5.

Figs 6 and 7 show the distribution of the relative velocities of stars inside OB-association, v'_l and v'_b, calculated with respect to its

Table 5. Expansion/compression of OB-associations with TGAS proper motions.

Name	p_l (km s^{-1} kpc^{-1})	p_b (km s^{-1} kpc^{-1})	a (pc)	e_1 (km s^{-1})	u_l (km s^{-1})	u_b (km s^{-1})	$\tilde{u}_l$ (km s^{-1}	$\tilde{u}_b$ (km s^{-1})	n_μ
SGR OB1	70 ± 38	238 ± 26	42	0.3 ± 0.1	2.9 ± 1.6	10.0 ± 1.1	2.6 ± 1.6	9.7 ± 1.1	13
CYG OB3	139 ± 138	159 ± 116	26	0.1 ± 0.0	3.6 ± 3.6	4.1 ± 3.0	3.5 ± 3.6	4.0 ± 3.0	15
CYG OB1	−57 ± 102	112 ± 131	32	0.3 ± 0.1	−1.8 ± 3.3	3.6 ± 4.2	−2.1 ± 3.3	3.3 ± 4.2	12
CYG OB8	−45 ± 55	186 ± 152	42	0.5 ± 0.1	−1.9 ± 2.3	7.7 ± 6.3	−2.4 ± 2.3	7.3 ± 6.3	10
CYG OB7	−39 ± 85	63 ± 26	53	0.8 ± 0.2	−2.1 ± 4.5	3.4 ± 1.4	−2.9 ± 4.5	2.6 ± 1.4	16
CEP OB2	77 ± 26	11 ± 26	45	1.1 ± 0.1	3.5 ± 1.2	0.5 ± 1.2	2.4 ± 1.2	−0.6 ± 1.2	34
CEP OB1	56 ± 19	1 ± 39	178	3.7 ± 0.1	9.9 ± 3.4	0.1 ± 6.9	6.2 ± 3.4	−3.6 ± 6.9	20
CEP OB3	−39 ± 48	71 ± 67	12	0.4 ± 0.0	−0.5 ± 0.6	0.9 ± 0.8	−0.9 ± 0.6	0.5 ± 0.8	12
PER OB1	45 ± 15	103 ± 22	59	1.4 ± 0.0	2.7 ± 0.9	6.1 ± 1.3	1.3 ± 0.9	4.7 ± 1.3	58
CAS OB6	9 ± 47	227 ± 80	78	1.9 ± 0.1	0.7 ± 3.7	17.8 ± 6.3	−1.2 ± 3.7	15.9 ± 6.3	11
CAM OB1	34 ± 20	3 ± 28	86	1.2 ± 0.2	2.9 ± 1.8	0.3 ± 2.4	1.7 ± 1.8	−0.9 ± 2.4	26
AUR OB1	−36 ± 27	19 ± 10	69	0.1 ± 0.3	−2.5 ± 1.9	1.3 ± 0.7	−2.6 ± 1.9	1.2 ± 0.7	12
MON OB2	−278 ± 77	232 ± 203	71	−1.3 ± 0.2	−19.7 ± 5.4	16.5 ± 14.4	−18.4 ± 5.4	17.8 ± 14.4	10
NGC 2439	64 ± 42	−106 ± 21	155	−2.8 ± 0.0	10.0 ± 6.6	−16.4 ± 3.2	12.8 ± 6.6	−13.6 ± 3.2	10
CAR OB1	118 ± 43	111 ± 28	63	0.2 ± 0.1	7.5 ± 2.7	7.0 ± 1.8	7.3 ± 2.7	6.8 ± 1.8	15
CAR OB2	−100 ± 136	42 ± 64	28	0.1 ± 0.0	−2.8 ± 3.8	1.2 ± 1.8	−2.9 ± 3.8	1.1 ± 1.8	10
CRU OB1	−29 ± 47	29 ± 23	40	0.1 ± 0.0	−1.2 ± 1.9	1.2 ± 0.9	−1.3 ± 1.9	1.1 ± 0.9	17
CEN OB1	−87 ± 33	35 ± 18	69	0.7 ± 0.1	−6.0 ± 2.3	2.4 ± 1.3	−6.7 ± 2.3	1.7 ± 1.3	27

average velocities v_{l0} and v_{b0}:

$$v'_l = 4.74 r \mu_l - v_{l0} \tag{37}$$

$$v'_b = 4.74 r \mu_b - v_{b0}. \tag{38}$$

Note that we excluded from consideration stars whose relative velocities exceed 50 km s^{-1}, i.e. $|v'_l| > 50$ or $|v'_b| > 50$ km s^{-1}: BD +57 530A (Per OB1), HD 212043 (Cep OB2), HD 192445 (Cyg OB3), HD 216878 (Cep OB3), BD +23 3843 (Vul OB1), HDE 328209 (Ara OB1B), HD 172488 (Sct OB2) and HD 112272 (Cen OB1). Stars BD +57 530A (Per OB1) and HD 212043 (Cep OB2) have parallaxes $\pi = 12.44 \pm 0.28$ and 4.91 ± 0.63, which correspond to distances $r = 0.1$ and 0.2 kpc, so they cannot belong to the associations Per OB1 and Cep OB2 located at distances $r = 1.8$ and 0.7 kpc, respectively. The parallaxes of other aforementioned stars are consistent with their membership in the corresponding associations. Generally, they can be binary or runaway stars that can form quite frequently in young clusters (e.g. Fujii & Portegies Zwart 2011).

Examination of Figs 6 and 7 shows that the suspected expansion/compression of some OB-associations is based on the velocities of a few stars, sometimes only one. For example, excluding only one of 10–11 stars from the associations Mon OB2 and NGC 2439 (HD 46573 from Mon OB2 and HD 63423 from NGC 2439) reduces the absolute values of the parameters of expansion/compression to the noise level. A similar situation is observed in Cen OB1, which demonstrates compression along l-coordinate, $p_l = -87 \pm 33$, at $P > 2.5\sigma$ confidence level. However, excluding 4 of 27 stars (HD 115363, HD 114340, HD 110946 and HD 116119) decreases $|p_l|$ to the noise level, $p_l = -24 \pm 20$ km s^{-1} kpc^{-1}.

We excluded from our consideration associations Mon OB2, NGC 2439 and Cen OB1 as having unreliable parameters of expansion/compression. The other three associations (Sgr OB1, Per OB1 and Car OB1) with $\tilde{u}_l$ and $\tilde{u}_b$, determined at $P > 2.5$ confidence level, demonstrate expansion.

Fig. 8 illustrates the expansion of the three OB-associations considered. It shows the linear increase of proper-motion components, μ_l or μ_b, with the corresponding coordinate, l or b, which suggests the expansion in the chosen direction (a decrease would indicate contraction). It can be seen that in all cases considered the spurious expansion determined by equation (34) is conspicuously smaller than the observed expansion.

Generally, the motion of OB-association as a whole in the sky plane with the tangential velocity V_t also affects the velocity distribution inside association by producing spurious compression in one part of association and spurious expansion in another part. The velocity of this spurious expansion/compression e_2 is determined by the following relation:

$$e_2 = V_t \frac{a^2}{2r^2} \tag{39}$$

with V_t in the following form:

$$V_t = 4.74 r \sqrt{\mu_l^2 + \mu_b^2}, \tag{40}$$

where μ_l and μ_b are given in Table 1. Formally, the velocity e_2 spuriously increases the velocity dispersion inside OB-association, but for OB-associations considered, e_2 does not exceed $e_2 < 0.1$ km s^{-1} and its contribution can be neglected.

4.2 Kinematic ages of OB-associations

We assume that all stars in an expanding OB-association started their motion at nearly the same time instant in the past and moved at nearly constant velocities; hence, their distances from the centre Δx and Δy are proportional to their observed velocities, $\Delta x = v'_l t$ and $\Delta y = v'_b t$. Though the distances and velocities are different for different stars, the time interval is supposed to be nearly the same for all stars in the OB-association considered. We estimate the so-called kinematic ages of expanding OB-associations by the formula:

$$T_l = (p_l f_v)^{-1}, \tag{41}$$

$$T_b = (p_b f_v)^{-1}, \tag{42}$$

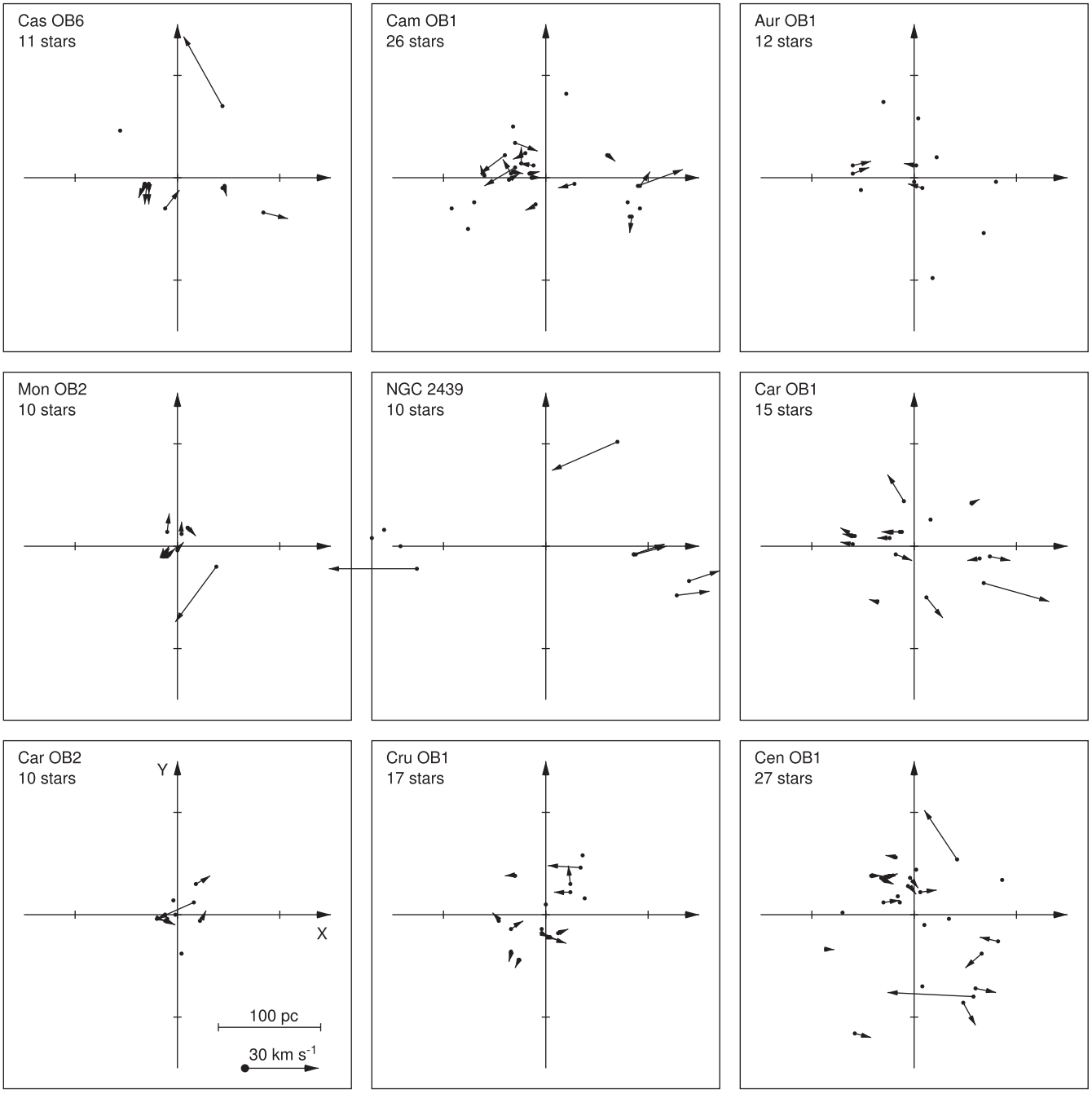

Figure 7. Distribution of the relative velocities v'_l and v'_b (equations 37 and 38) inside OB-associations with more than 10 TGAS stars. See caption to Fig. 6 for more details.

where factor $f_v = 3.16/3.09 \times 10^{-3}$ transforms velocities in units of km s^{-1} into kpc Myr^{-1}. The errors in T_l and T_b are determined by errors in p_l and p_b, respectively.

Table 6 lists different estimates of the kinematic expansion ages of the three OB-associations considered. We can see that the T_l and T_b ages lie in the interval 4–10 Myr.

Here, we ignore the epicyclic motions, which, through Coriolis forces, change the direction of residual velocities (those superimposed on the Galactic rotation). This concerns only velocities in the Galactic plane. The Galactic rotation curve is nearly flat, and hence the epicyclic frequency at the solar distance is $\kappa = \sqrt{2}\Omega_0$ or 43 km s^{-1} kpc^{-1}, and one quarter of the epicyclic period amounts to 37 Myr. It is this time interval that takes the Coriolis force to change the direction of residual velocities by 90°. We can see that the average age of OB-stars, ∼10 Myr, amounts to ∼30 per cent of one quarter of the epicyclic period. However, epicyclic motions change the direction of expansion but they do not prevent it. So the value of p_l is determined by some combination of the expansion in l-direction and that in the perpendicular direction – along the line of sight. Parameter p_l should rather be viewed as characterizing

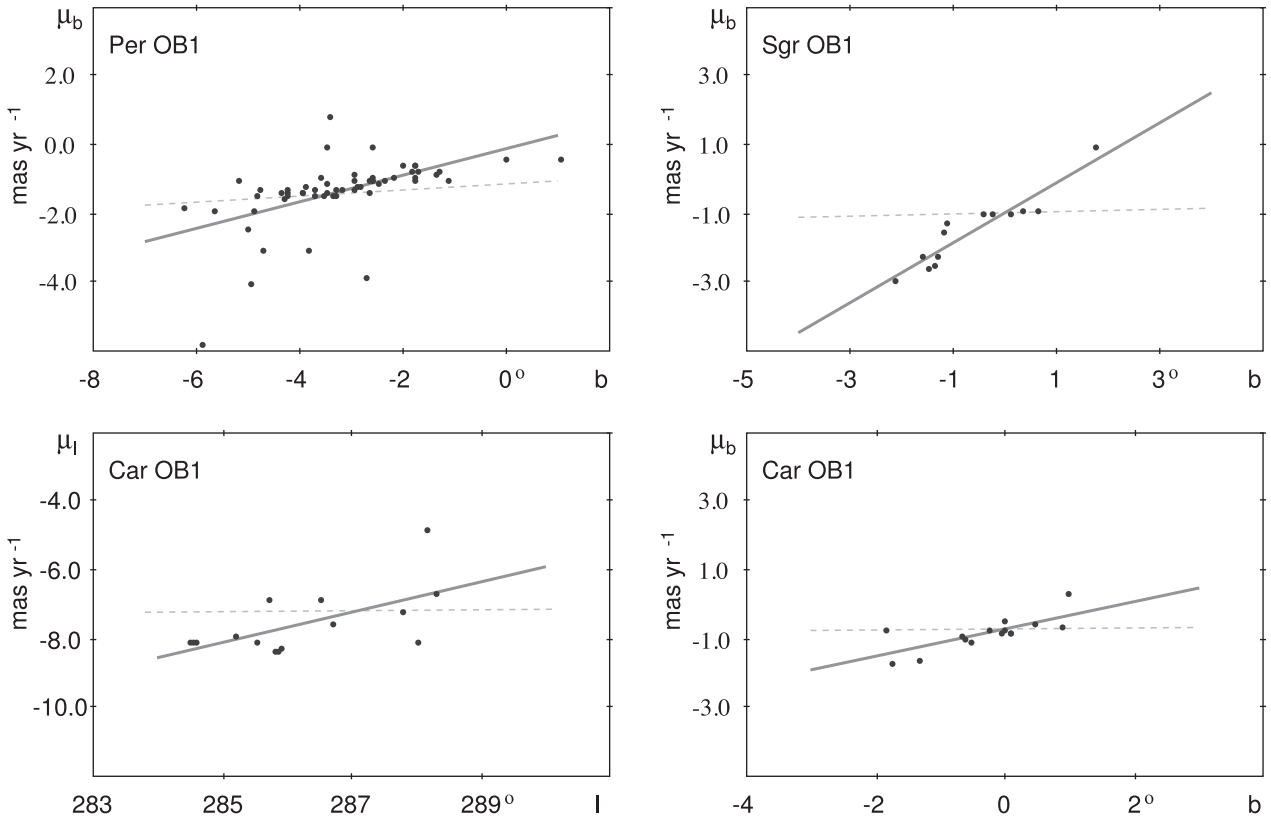

Figure 8. Dependence of the proper motions μ_l or μ_b on the corresponding Galactic coordinates, l or b, calculated for TGAS stars in associations Per OB1, Sgr OB1 and Car OB1. The solid line indicates the observed linear dependence. The increase of proper-motion component along the corresponding coordinate indicates expansion in the chosen direction. The thin dashed line displays the contribution of spurious expansion due to line-of-sight velocity V_r (equation 34). In all cases considered the spurious expansion is conspicuously smaller than the observed expansion.

Table 6. Kinematic ages of OB-associations.

Name	T_l (Myr)	T_b (Myr)	T_l^* (Myr)	T_b^* (Myr)
PER OB1	–	$9.5^{+2.5}_{-1.7}$	–	$8.9^{+7.6}_{-3.4}$
CAR OB1	$8.3^{+4.7}_{-2.2}$	$8.8^{+4.7}_{-2.2}$	<10	$7.4^{+1.1}_{-5.1}$
SGR OB1	–	$4.1^{+0.5}_{-0.4}$	–	$3.3^{+2.7}_{-3.3}$

the expansion in the Galactic plane. Here, we do not consider the expansion along the line of sight because with TGAS data the accuracy of sky-plane velocity components is for the first time better than that of line-of-sight velocities.

There is also another method to determine the time in the past when OB-associations had minimal sizes (see also Brown et al. 1997). We trace back the positions of stars in OB-association using their relative velocities v_l' and v_b':

$$x(t) = x_0 - v_l' t, \tag{43}$$

$$y(t) = y_0 - v_b' t, \tag{44}$$

where x_0 and y_0 are the observed coordinates of TGAS stars with respect to the centre of OB-association, and compute the sizes of the most compact parts of OB-association at different time instants. The sizes, s_l(t) and s_b(t), containing 50 per cent of TGAS stars of the corresponding OB-association are calculated in the following way. We sort the coordinates of association member stars, x and y, in the ascending order and seek the subset $S = \{j+1, j+2, ..., j+k\}$ containing $k = n_\mu/2$ stars (where n_μ is the number of TGAS stars in OB-association) having the smallest span in the corresponding coordinate, x_{j+k}–x_{j+1} and y_{j+k}–y_{j+1}. These minimal spans in the x- and y-direction give the values of $s_l(t)$ and $s_b(t)$, respectively. That is done to mitigate the effect of individual stars.

Fig. 9 shows the dependence of s_b and s_l on the time t in the past. We consider only OB-associations Per OB1, Car OB1 and Sgr OB1 with well-determined parameters $\tilde{u}_l$ or $\tilde{u}_b$. The curves s_b(t) and s_l(t) are often indented and some of them have several local minima, which are due to abrupt changes of the estimated size due to inclusion/exclusion of individual stars in the half-member minimal-span subset. We determine the kinematic expansion ages of OB-associations, T_b^* and T_l^*, as the time instants t in the past corresponding to the minimal values of s_b and s_l, respectively (Fig. 9). However, in some cases, we can give only an upper estimate for the kinematic age.

Table 6 lists the inferred T_l^* and T_b^* ages and their errors, which are calculated through the distances, Δx and Δy, in the l- and b-direction that stars pass due to their errors in proper motions, $\varepsilon_{\mu l}$ and $\varepsilon_{\mu b}$, during the time intervals T_l^* and T_b^*, respectively:

$$\Delta x = 2\ 4.74 r \varepsilon_{\mu l}\ T_l^*\ f_v, \tag{45}$$

$$\Delta y = 2\ 4.74 r \varepsilon_{\mu b}\ T_b^*\ f_v, \tag{46}$$

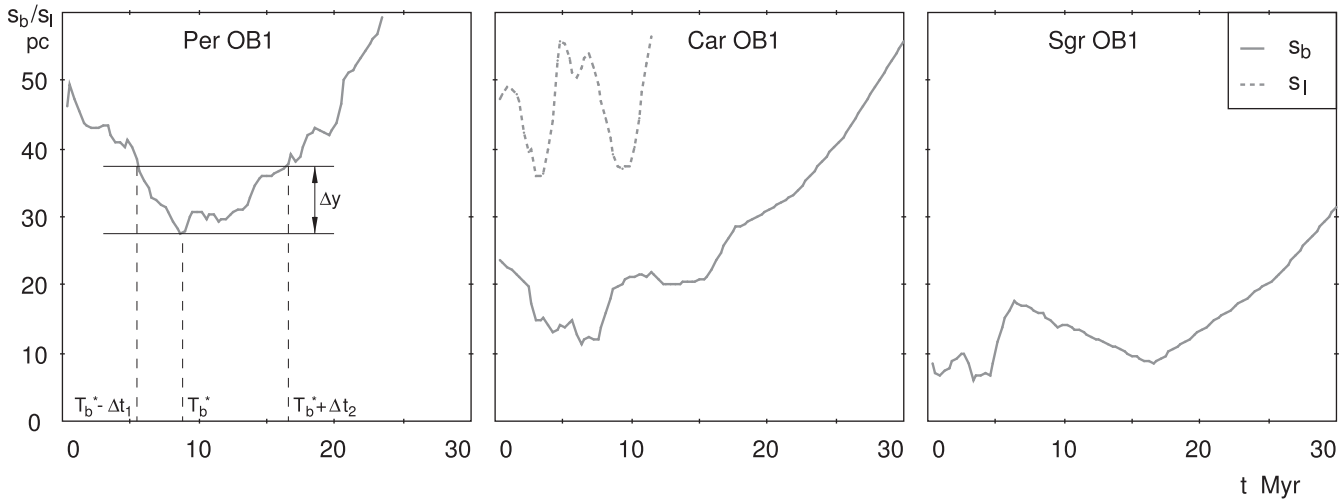

Figure 9. Dependence of the half-member size of OB-association in the *b*- or *l*-direction, s_b or s_l, on the time t in the past. Here, s_b and s_l are the lengths of the minimal intervals containing 50 per cent of members of OB-associations, n_μ, at the corresponding time moments. The positions of stars at each time instant were calculated by equations (43) and (44). Only OB-associations with well-determined parameters of expansion are considered. We illustrate the method of deriving errors in kinematic ages, Δt_1 and Δt_2, with the example of the Per OB1 association: a horizontal line $y = s_b(T_b^*) + \Delta y$ intersects the curve $s_b(t)$ at two points with abscissae of $T_b^* - \Delta t_1$ and $T_b^* + \Delta t_2$, where Δt_1 and Δt_2 are error estimates on the left and right of the minimum.

where $\varepsilon_{\mu l}$ and $\varepsilon_{\mu b}$ are in mas yr^{-1} but Δx, Δy and r are in kpc. Factor two reflects possible changes of the sizes of OB-association at left and right sides of the distribution. The average errors in proper motions, $\varepsilon_{\mu l}$ and $\varepsilon_{\mu b}$, lie in the range of 0.05–0.07 mas yr^{-1}. The distances Δx and Δy increase with increasing the distance to the OB-association, r, and with increasing kinematic ages, T_l^* or T_b^*. They have the following values: $\Delta y = 10$ pc (Per OB1), $\Delta x \approx \Delta y = 7$–10 pc (Car OB1) and $\Delta y = 4$ pc (Sgr OB1).

To transform errors in distances, Δx and Δy, into errors in time intervals, Δt_1 and Δt_2, we use following expressions:

$$s_l(T_l^*) + \Delta x = s_l(T_l^* - \Delta t_1) = s_l(T_l^* + \Delta t_2), \quad (47)$$

$$s_b(T_b^*) + \Delta y = s_b(T_b^* - \Delta t_1) = s_b(T_b^* + \Delta t_2), \quad (48)$$

where Δt_1 and Δt_2 are the errors estimated on the left and right of the minimum on the curves $s_l(t)$ or $s_b(t)$. To illustrate this method, we chose association Per OB1 and drew a horizontal line with the ordinate $y = s_b(T_b^*) + \Delta y$ that intersects the curve $s_b(t)$ at two points with abscissae of $T_b^* - \Delta t_1$ and $T_b^* + \Delta t_2$ (Fig. 9).

Table 6 shows that the kinematic ages of OB-associations obtained by two different methods, T_l and T_l^* or T_b and T_b^* agree with each other within the errors. The kinematic ages, T_l, T_l^*, T_b and T_b^*, determined by both methods for three OB-associations considered lie in the range of 3–10 Myr. These estimates do not exceed the main-sequence ages of O–B2 stars, $T_s < 30$ Myr (Bressan et al. 2012).

4.3 Minimal sizes of OB-associations in the past

The second method is also interesting because it gives us the estimates of the minimal sizes of OB-associations corresponding to the time instants T_l^* and T_b^* (Fig. 9). The minimal sizes of the most compact parts of OB-associations containing 50 per cent of star-members, $s_l(T_l^*)$ and $s_b(T_b^*)$, appear to be 27 pc for Per OB1, 11–36 pc for Car OB1 and 6 pc for Sgr OB1.

Fig. 9 shows that sizes of Per OB1 and Car OB1 in latitude directions, s_b, were nearly twice smaller in the past than nowadays. The formula for the virial mass (equation 20) includes the radius of the system a referred to the epoch of star formation and we therefore should correct their virial masses $M_{\rm vir}$. Assuming that the contributions to a^2 from the coordinates x and y are nearly the same, we must reduce $M_{\rm vir}$ of Per OB1 and Car OB1 by the factor $(1 + 0.25)/2)^{1/2} = 0.79$ and upscale star-formation efficiency ϵ by a factor of 1.26 to the new values of 4.4 and 1.8 per cent, respectively.

We can see that the minimal sizes of the Per OB1 and Car OB1 associations lie in the range of 11–27 pc and are consistent with diameters of giant molecular clouds, 10–80 pc. As for Sgr OB1, the situation is unclear here: we see too quick expansion in very small area. Moreover, it contains only 13 stars with known TGAS proper motions and errors of their μ_b are the highest, $\varepsilon_{\mu b} = 0.07$ mas yr^{-1}, amongst stars in the OB-associations considered.

Possibly, the quick expansion of Sgr OB1, as well as the large velocity dispersion in Cyg OB7 and Cyg OB8 have the same origin – larger errors of proper motions in fields rich in bright stars.

4.4 Expansion of per OB1

Let us consider the expansion of the per OB1 association in more detail (Fig. 10). It exhibits significant expansion along *b*-coordinates, $p_b = 103 \pm 22$ km s^{-1} kpc^{-1} (Table 5). However, the expansion can be even faster if we tilt the coordinate axes (x, y) by the angle $\alpha = 26^\circ$ with respect to the Galactic plane. In the new reference frame (x', y'), the expansion parameter has the values of $p'_y = 136 \pm 25$ kpc^{-1} corresponding to the velocity 7.5 km s^{-1}. Interestingly, the new axis x' is nearly parallel to the line connecting two rich open clusters NGC 869 ($l = 134.63^\circ$, $b = -3.74^\circ$) and NGC 884 ($l = 135.07^\circ$, $b = -3.59^\circ$) also known as the double cluster *h* and χ Persei lying practically at the centre of OB-association Per OB1. So the maximal expansion happens in the direction nearly perpendicular to the main plain of the double cluster.

We subdivide stars of Per OB1 into two groups: red supergiants of spectral type K and M (nine objects with TGAS proper motions) and stars of type O-B (49 objects). The ages of red supergiants must be less than 50 Myr, while those of the main-sequence O-B2 stars must be less than 30 Myr (Bressan et al. 2012). However, we do not see difference in their kinematical behaviour: both groups take

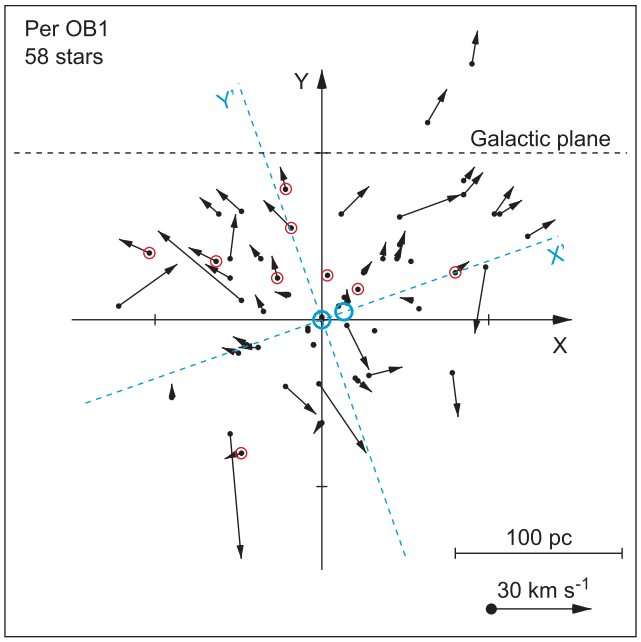

Figure 10. Distribution of relative velocities v'_l and v'_b in the Per OB1 association. Axes x and y are directed towards increasing values of Galactic coordinates l and b, respectively. Two open clusters NGC 869 ($l = 134.63°$, $b = -3.74°$) and NGC 884 ($l = 135.07°$, $b = -3.59°$) lying practically in the centre of the OB-association are shown as circles (coloured blue in electronic edition). The line connecting them (the dashed line) is tilted by 20° to the Galactic plane. The expansion of Per OB1 ($p = 136 \pm 25$ km s^{-1} kpc^{-1}) is the fastest in the direction nearly perpendicular to this line. The supergiants of type K and M are outlined by circles (coloured red in electronic edition). The position of the Galactic plane is shown by the black dashed line.

part in the expansion along l- and b-directions. The parameters of expansion obtained for red supergiants exclusively are $p_l = 75 \pm 15$ and $p_b = 61 \pm 14$ km s^{-1} kpc^{-1}, while those derived for OB-stars only are $p_l = 35 \pm 18$ and $p_b = 109 \pm 26$ km s^{-1} kpc^{-1}. These parameters are consistent within 1.2σ. Probably, red supergiants and OB stars observed in Per OB1 have very close ages and take part in the same expansion.

Cappa & Herbstmeier (2000) notice that there is a lot of neutral hydrogen and no molecular gas in the vicinity of the Per OB1 association. They found a lot of H I bubbles surrounding massive WR and Of stars there.

Note that the evolutionary ages of clusters h and χ Persei are comparable to those of stars in OB-associations, 10 Myr (Dias et al. 2002; Kharchenko et al. 2013) and the inferred expansion age of the association. Possibly, the expansion of Per OB1 and formation of double stellar cluster h and χ Persei in its centre have the same cause – the quick loss of gas in their parent giant molecular cloud.

As for double clusters, Kroupa et al. (2001) find multiple clusters in some of their simulations of the formation of bound clusters inside the expanding OB-associations. Though their models are very compact, ∼10 pc, the physical mechanism considered can be universal. The authors explain the formation of double clusters in their models by gravitational interactions between neighbour stars, which cause the redistribution of the velocity dispersion from the radial direction into the azimuthal one. This mechanism can lead to the formation of a subsystem with non-zero angular momentum about the origin of the expanding flow.

5 CONCLUSIONS

We have studied the kinematics of OB-associations identified by Blaha & Humphreys (1989) using the stellar proper motions from the TGAS catalogue (Michalik et al. 2015). The average difference in the median proper potions of OB-associations obtained with TGAS and Hipparcos data is 0.67 mas yr^{-1}, which is comparable to the average error of Hipparcos proper motions, 0.916 mas yr^{-1}, for stars of OB-associations.

Generally, the results based on TGAS and Hipparcos catalogues demonstrate a good agreement. The parameters of the Galactic rotation curve obtained with TGAS (Table 2) and Hipparcos (Mel'nik & Dambis 2009) proper motions agree within the errors. The same can be said about residual velocities ($V_{\rm res} = V_{\rm obs} - V_{\rm rot} - V_{\rm ap}$) of OB-associations in stellar–gas complexes identified by Efremov & Sitnik (1988). The rms deviation of the velocities of OB-associations from the Galactic rotation curve amounts $\sigma_0 = 7.2$–7.5 km s^{-1}. This value is nearly the same whether computed with TGAS or Hipparcos data, suggesting that the residual velocities of 7–8 km s^{-1} are real and not an artefact.

When computed with TGAS data, the rms deviation of the velocities of OB- associations in the z-direction is $\sigma_{vz} = 2.7$ km s^{-1}, which is considerably less than the scatter obtained with Hipparcos data, $\sigma_{vz} = 5.0$ km s^{-1}.

We found a considerable decrease, by a factor of 0.4, in the velocity dispersions inside 18 OB-associations containing more than 10 TGAS stars compared to the values derived with Hipparcos data. The average one-dimensional velocity dispersion inside OB-associations computed with TGAS catalogue data is $\overline{\sigma_v} = 3.9$ km s^{-1}.

The effective contribution from binary OB-stars into the velocity dispersion σ_v inside OB-associations is $\sigma_b = 1.2$ km s^{-1}.

The virial $M_{\rm vir}$ and stellar $M_{\rm st}$ masses of 18 OB-associations considered have the median values of 7.1×10^5 and 9.0×10^3 $M_\odot$, respectively. Generally, the virial mass exceeds the stellar mass by more than 70 times. This fact together with assumption that the volumes of OB-associations do not contain a lot of dense gas supports the conclusion that they are unbound objects.

The star-formation efficiency ϵ in OB-associations varies from 0.1 to 13.6 per cent with the median of $\epsilon = 2.1$ per cent, which agrees with other estimates (Myers et al. 1986; Evans et al. 2009; Garcia et al. 2014).

We determined the tidal radii of OB-associations under two assumptions: (1) OB-associations include neutral gas and its mass is proportional to the volume of the association, so that the present-day mass of the OB-association consists of masses of the gas and stellar components; (2) the masses of OB-associations are determined by their stellar component exclusively. In the first case, the median tidal radius appears to be 40 pc, suggesting that 27 per cent of member stars of OB-associations are located outside their tidal radii. In the second case, the tidal radii range from 14 to 48 pc with the median value of 26 pc, implying that 39 per cent of stars of OB-associations must lie outside their tidal radii. Thus, ∼1/3 of stars of OB-associations must lie outside their tidal radius.

The high accuracy of TGAS proper motions allowed us to find the expansion inside the OB-associations Per OB1 and Car OB1, supporting the idea that they are unbound objects. The velocity of expansion amounts, on average, to 6.3 km s^{-1} (Table 5).

We corrected the observed specific velocities of expansion/compression, u_l and u_b, for the effect of spurious expansion/compression caused by the motion of OB-association as a whole with the line-of-sight velocity V_r (equation 34). Only cases

with well-determined corrected velocities, $\tilde{u}_l$ and $\tilde{u}_b$, are considered (Table 5).

The kinematic ages of the expanding OB-associations Per OB1 and Car OB1 (time moments in the past when they had their minimal sizes) calculated by two methods are 7–10 Myr. The minimal diameter of the most compact parts of these OB-associations in the past lies in the range of 11–27 pc that is comparable to the diameters of Galactic giant molecular clouds, 10–80 pc (Sanders et al. 1985).

We studied in more detail the expansion of the Per OB1 association. The direction of its fastest expansion (Y' in Fig. 10) appears to be tilted by 26° with respect to the b-direction and is nearly perpendicular to the plane determined by the positions of the two rich open clusters, h and χ Persei, lying in the centre of the association. We found no significant difference between the parameters of expansion derived for OB-stars and red supergiants in this association.

ACKNOWLEDGEMENTS

We thank A. G. A. Brown for fruitful discussion. We thank A. S. Rastorguev and O. K. Sil'chenko for useful remarks and suggestions. This work has made use of data from the ESA mission *Gaia* (https://www.cosmos.esa.int/gaia), processed by the *Gaia* Data Processing and Analysis Consortium (DPAC; https://www.cosmos.esa.int/web/gaia/dpac/consortium). Funding for the DPAC has been provided by national institutions, in particular the institutions participating in the *Gaia* Multilateral Agreement. This research has made use of the VizieR catalogue access tool, CDS, Strasbourg, France. The original description of the VizieR service was published by Ochsenbein, Bauer & Marcout (2000). Analysis of observational data was supported by Russian Scientific Foundation grant no. 14-22-00041.

REFERENCES

Aldoretta E. J. et al., 2015, AJ, 149, 26
Ambartsumian V. A., 1949, Soviet Astron. Zhurn., 26, 3
Barbier-Brossat M., Figon P., 2000, A&AS, 142, 217
Baumgardt H., Kroupa P., 2007, MNRAS, 380, 1589
Blaauw A., 1964, ARA&A, 2, 213
Blaha C., Humphreys R. M., 1989, AJ, 98, 1598
Bobylev V. V., Baikova A. T., 2012, Astron. Lett., 38, 638
Boehle A. et al., 2016, ApJ, 830, 17
Boily C. M., Kroupa P., 2003a, MNRAS, 338, 665
Boily C. M., Kroupa P., 2003b, MNRAS, 338, 673
Branham R. L., 2017, Ap&SS, 362, 29
Bressan A., Marigo P., Girardi L., Salasnich B., Dal Cero C., Rubele S., Nanni A., 2012, MNRAS, 427, 127
Brown A. G. A., Dekker G., de Zeeuw P. T., 1997, MNRAS, 285, 479
Cappa C. E., Herbstmeier U., 2000, AJ, 120, 1963
Colín P., Vázquez-Semadeni E., Gómez G. C., 2013, MNRAS, 435, 1701
Dale J. E., Ercolano B., Bonnell I. A., 2012, MNRAS, 427, 2852
Dambis A. K., Mel'nik A. M., Rastorguev A. S., 1995, Astron. Lett., 21, 291
Dambis A. K., Mel'nik A. M., Rastorguev A. S., 2001, Astron. Lett., 27, 58
Dambis A. K., Berdnikov L. N., Kniazev A. Y., Kravtsov V. V., Rastorguev A. S., Sefako R., Vozyakova O. V., 2013, MNRAS, 435, 3206
de Zeeuw P. T., Hoogerwerf R., de Bruijne J. H. J., Brown A. G. A., Blaauw A., 1999, AJ, 117, 354
Dias W. S., Alessi B. S., Moitinho A., Lépine J. R. D., 2002, A&A, 389, 871
Efremov, Yu. N., Sitnik T. G., 1988, Soviet Astron. Lett., 14, 347
Elmegreen B. G., 1983, MNRAS, 203, 1011
ESA 1997, The HIPPARCOS and TYCHO catalogues. Astrometric and photometric star catalogues derived from the ESA HIPPARCOS Space Astrometry Mission, ESA SP, 1200
Evans N. J. et al., 2009, ApJS, 181, 321
Feast M. W., Laney C. D., Kinman T. D., van Leeuwen F., Whitelock P. A., 2008, MNRAS, 386, 2115
Francis, Ch., Anderson E., 2014, MNRAS, 441, 1105
Franco J., Shore S. N., Tenorio-Tagle G., 1994, ApJ, 436, 795
Fujii M. S., Portegies Zwart S., 2011, Sci., 334, 1380
Gaia Collaboration et al., 2016a A&A, 595, A1
Gaia Collaboration et al., 2016b A&A, 595, A2
Garcia P., Bronfman L., Nyman L.-A., Dame T. M., Luna A., 2014, ApJS, 212, 2
Garmany C. D., Stencel R. E., 1992, A&AS, 94, 211
Glushkova E. V., Dambis A. K., Mel'nik A. M., Rastorguev A. S., 1998, A&A, 329, 514
Goldreich P., Tremaine S., 1980, ApJ, 241, 425
Groenewegen M. A. T., Udalski A., Bono G., 2008, A&A, 481, 441
Grosbol P., 2016, A&A, 585, 141
Grossman A. S., Graboske H. C., Jr, 1971, ApJ, 164, 475
Hills J. G., 1980, ApJ, 225, 986
Hog E. et al., 2000, A&A, 355, L27
Hohle M. M., Neuhäuser R., Schutz B. F., 2010, Astron. Nachr., 999, 789
Humphreys R. M, McElroy D. B., 1984, ApJ, 284, 565
Kharchenko N. V., Piskunov A. E., Schilbach E., Röser S., Scholz R.-D., 2013, A&A, 558, 53
Kim J.-G., Kim W.-T., Ostriker E. C., 2016, ApJ, 819, 137
Kroupa P., 2002, Sci. 295, 82
Kroupa P., Aarseth S., Hurley J., 2001, MNRAS, 321, 699
Krumholz M. R., Matzner C. D., McKee C. F., 2006, ApJ, 653, 361
Larson R. B., 1981, MNRAS, 194, 809
Lindegren L. et al., 2016, A&A, 595, A4
Mac Low M.-M., Klessen R. S., 2004, Rev. Mod. Phys., 76, 125
Madsen S., Dravins D., Lindegren L., 2002, A&A, 381, 446
Mason B. D., Gies D. R., Hartkopf W. I., Bagnuolo W. G., ten Brummelaar T., McAlister H. A., 1998, AJ, 115, 821
McKee C. F., 1989, ApJ, 345, 782
McKee C. F., Ostriker E. C., 2007, ARA&A, 45, 565
Mel'nik A. M., Dambis A. K., 2009, MNRAS, 400, 518
Mel'nik A. M., Rautiainen P., 2009, Astron. Lett., 35, 609
Mel'nik A. M., Rautiainen P., 2011, MNRAS, 418, 2508
Mel'nik A. M., Efremov, Yu. N., 1995, Astron. Lett., 21, 10
Mel'nik A. M., Dambis A. K., Rastorguev A. S., 1999, Astron. Lett., 25, 518
Mel'nik A. M., Dambis A. K., Rastorguev A. S., 2001, Astron. Lett., 27, 521
Mel'nik A. M., Rautiainen P., Berdnikov L. N., Dambis A. K., Rastorguev A. S., 2015, AN, 336, 70
Mel'nik A. M., Rautiainen P., Glushkova E. V., Dambis A. K., 2016, Ap&SS, 361, 60
Michalik D., Lindegren L., Hobbs D., 2015, A&A, 574, 115
Myers P. C., Dame T. M., Thaddeus P., Cohen R. S., Silverberg R. F., Dwek E., Hauser M. G., 1986, ApJ, 301, 398
Nikiforov I. I., 2004, in Byrd G. G., Kholshevnikov K. V., Myllri A. A., Nikiforov I. I., Orlov V. V., eds, ASP Conf. Ser. Vol. 316, Order and Chaos in Stellar and Planetary Systems. Astron. Soc. Pac., San Francisco, p. 199
Ochsenbein F., Bauer P., Marcout J., 2000, A&AS, 143, 23
Press W. H., Flannery B. P., Teukolsky S. A., Wetterling W. T., Kriz S., 1987, Numerical Recipes: The Art of Scientific Computing. Cambridge Univ. Press, Cambridge
Rastorguev A. S., Pavlovskaya E. D., Durlevich O. V., Filippova A. A., 1994, Astron. Lett., 20, 591

Rautiainen P., Mel'nik A. M., 2010, A&A, 519, 70
Reid M. J. et al., 2009a, ApJ, 700, 137
Reid M. J., Menten K. M., Zheng X. W., Brunthaler A., Xu Y., 2009b, ApJ, 705, 1548
Sana H., 2017, Proc. IAU Symp. 329, in press (arXiv:170301608)
Sanders D. B, Scoville N. Z., Solomon P. M., 1985, ApJ, 289, 373
Sitnik T. G., Mel'nik A. M., 1996, Astron. Lett., 22, 422
Solomon P. M., Rivolo A. R., 1989, ApJ, 339, 919
Solomon P. M., Rivolo A. R., Barrett J., Yahil A., 1987, ApJ, 319, 730
Stark A. A., Blitz L., 1978, ApJ, 225, 15
Tutukov A. V., 1978, A&A, 70, 57
Vine S. G., Bonnell I. A., 2003, MNRAS, 342, 314
Zinnecker H., Yorke H. W., 2007, ARA&A, 45, 481

SUPPORTING INFORMATION

Supplementary data are available at *MNRAS* online.

Table 2. Spectral, photometric and kinematic data for stars in OB-associations.

Please note: Oxford University Press is not responsible for the content or functionality of any supporting materials supplied by the authors. Any queries (other than missing material) should be directed to the corresponding author for the article.

This paper has been typeset from a TEX/LATEX file prepared by the author.